Failure mechanism of one-way slabs under concentrated loads after local reinforcement yielding

de Sousa, Alex M.D.; Lantsoght, Eva O.L.; El Debs, Mounir K.

DOI
10.1016/j.engstruct.2023.116396

Publication date
2023

Document Version
Final published version

Published in
Engineering Structures

Engineering Structures 291 (2023) 116396

Contents lists available at ScienceDirect

Engineering Structures

journal homepage: www.elsevier.com/locate/engstruct

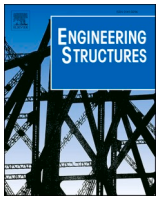

Failure mechanism of one-way slabs under concentrated loads after local reinforcement yielding

Alex M.D. de Sousa [a,*], Eva O.L. Lantsoght [b,c], Mounir K. El Debs [d]

[a] Postdoctoral Fellow, University of São Paulo, São Carlos School of Engineering, São Carlos, Brazil
[b] Universidad San Francisco de Quito, Quito, Ecuador
[c] Delft University of Technology, Delft, The Netherlands
[d] University of São Paulo, São Carlos School of Engineering, São Carlos, Brazil

ARTICLE INFO

Keywords:
One-way shear
Punching shear
Flexure
Concentrated load
One-way slabs
Reinforcement yielding
Code provisions
Extended strip model

ABSTRACT

One-way slabs under concentrated loads may fail by one-way shear such as wide beams, punching shear, flexure, or by combining two or more of these mechanisms. Nevertheless, most publications have only addressed shear and punching failures without flexural reinforcement yielding. This study investigates the ultimate shear capacity of one-way slabs under concentrated loads with local reinforcement yielding. In total, 12 tests were conducted on six reinforced concrete slabs. Simply supported slabs of 1.60 m × 3.40 m × 0.15 m were tested. Three parameters were varied: the load position, the span length and the reinforcement ratio. All slabs failed initially by punching with limited or extensive reinforcement yielding. Due to the relatively large amount of transverse reinforcement (0.44 %), most slabs underwent a large shear redistribution around the load, resulting in a wide beam shear failure after the local punching failure. The test results were compared to the theoretical predictions of shear, punching and flexure capacity using code expressions and the Extended Strip Model (ESM). The ESM resulted in the closest predictions of the experiments. These experiments confirm that a brittle shear and punching failure mechanism can occur even after extensive reinforcement yielding. Moreover, the results indicate that the ESM can be used to assess one-way slabs under concentrated loads with local reinforcement yielding.

1. Introduction

One-way slabs under large concentrated loads are commonly found on parking floors, bridge decks, industrial floors, and residential building floors [1–4]. For parking floors or bridge decks, the live load position is variable. Different failure mechanisms may govern for a given slab depending on the load position and other parameters, such as the slab width [5]. For instance, when the slab width b_{slab} is not large compared to the load size in the width direction l_{load}, the slab may fail as a wide beam in one-way shear [6,7] (Fig. 1a). At the same time, when the load is placed close to the support or the slab width is considerably larger than the load size, the shear flow around the load becomes predominantly radial and, hence, the punching failure may occur (Fig. 1b). The same shear stress distribution occurs when the distance from the load to the support increases [8]. Since the entire slab width b_{slab} does not always contribute effectively to the sectional shear capacity, a slab strip of effective shear width (b_{eff} - Fig. 1b) is commonly defined to evaluate the one-way shear capacity [1] for such slabs. The effective shear width is commonly defined as the width on which the maximum shear stress v_{max} integrated along this width b_{eff} equals the total shear force V_E along the slab width (Fig. 1b).

Most experimental studies on one-way slabs under concentrated loads focused on the one-way shear and punching shear capacity of tests without any reinforcement yielding at failure [1,2,8–10]. Investigations related to combined failure mechanisms between flexure and punching were conducted on slab-column connections or flat slabs under concentric loads, exploring this combination of failure modes for two-way slabs [11,12]. However, investigations related to one-way slabs under concentrated loads presenting local reinforcement yielding or at the transition between shear and flexural failure mechanisms were not often discussed [13]. In practice, design codes such as ACI 318-19 [14] are based on the premise that a slab should fail in flexure before it fails in shear or punching. In this context, it is likely that at failure due to an unexpected overload (for instance), a properly designed slab develops significant reinforcement yielding before a shear or punching failure

* Corresponding author.
E-mail address: alex_dantas@usp.br (A.M.D. de Sousa).

https://doi.org/10.1016/j.engstruct.2023.116396
Received 23 February 2023; Received in revised form 5 May 2023; Accepted 30 May 2023
Available online 17 June 2023

Notations

a	shear span: distance between the center of the support and the center of the load
a_v	clear shear span: distance between face of support and face of load
b_0	total length of the shear resisting control perimeter
b_{eff}	effective shear width for one-way shear resistance analyses
$b_{eff,french}$	French effective shear width
b_{load}	size of the concentrated load in the slab width direction (transverse direction)
b_r	distance between free edge and center of load along the width direction
b_{slab}	slab width
d_{avg}	average effective depth of the flexural reinforcement
d_l	effective depth towards longitudinal steel
d_t	effective depth towards transverse steel
f_{ck}	characteristic concrete compressive strength
f_{cm}	average compressive strength measured on cylinder specimens
f_{ctd}	design value of the concrete tensile strength
$f_{ctk,inf}$	characteristic tensile strength of the concrete in the lower quantile
f_{yi}	steel yielding stress in the evaluated direction (x = longitudinal direction and y = transverse direction)
h_{slab}	slab thickness
k_1	factor accounting for axial forces in one-way shear for EN 1992-1-1:2004 [17]
k_{CEN}	constant accounting for size effect in one-way shear for EN 1992-1-1:2004 [17]
l_{edge}	length of the strip between the load and the edge (in the transverse direction)
l_{load}	size of the concentrated load in the span direction
l_{span}	span length
l_w	loaded length of the strip close to the free edge
$m_{sag,x}$	sagging yielding moment per unit length in the direction x
$m_{sag,y}$	sagging yielding moment per unit length in the direction y
$r_{s,ij}$	distance between the center of the concentrated load and the point of contraflexure in the evaluated direction (CSCT model)
v	shear stress (nominal shear force)
v_E	shear stress at the control section
v_{Ed}	design shear stress at the control section
v_{min}	minimum one-way shear resistance in NEN 1992-1-1:2005 [17]
$v_{Rd,CEN}$	nominal one-way shear resistance for NEN 1992-1-1:2005 [17]
$v_{R,punch}$	unitary shear capacity for two-way shear (punching)
$v_{R,punch,net}$	net shear capacity for two-way shear considering the self-weight effect for punching
$v_{R,shear}$	unitary shear capacity for one-way shear
v_g	shear forcer per unit length in the control section due to the self-weight
$w_{ACI,x}$	one-way shear capacity based on dl given by ACI318-14
$w_{ACI,y}$	one-way shear capacity based on dt given by ACI318-14
A_s	cross-sectional area of flexural reinforcement
$C_{Rd,c}$	calibration factor for design in the shear and punching shear expressions of NEN 1992-1-1:2005 [17]
$C_{R,c,test}$	calibration factor recommended = 0.15 for comparison with data test
F	applied concentrated load
F_{flex}	predicted concentrated load that causes a flexural failure according to yield line analyses
$F_{predicted,shear}$	predicted concentrated load that causes a one-way shear failure
$F_{predicted,punch}$	predicted concentrated load that causes a punching shear failure
F_{test}	applied concentrated load at failure
L	span length between two supports for simply supported slabs and the largest distance between the farthest support from the load and the point of contraflexure for loads close to continuous support (definition applied for the Extended Strip Model)
$M_{sag,x}$	sagging moment capacity in the x-direction (span direction, tensile in the bottom reinforcement)
$M_{sag,y}$	sagging moment capacity in the y-direction (transverse direction, tensile in the bottom reinforcement)
M_{span}	sagging moment in the span caused by all loads on the slab
M_{sup}	hogging moment over the support caused by all loads on the slab
$M_{hog,x}$	hogging moment capacity in the x-direction (span direction, tensile in the top reinforcement)
$M_{hog,y}$	hogginh moment capacity in the y-direction (transverse direction, tensile in the top reinforcement)
P_{test}	approximately the maximum load applied at the concentrated load in the experiments
P_{edge}	capacity of strip between load and free edge
P_{ESM}	maximum load according to the Extended Strip Model
P_{line}	resultant of line load, maximum value
P_{sup}	capacity of strip between load and support
P_x	capacity of a strip in the back side of the load (x-direction)
P_y	capacity of a strip in the y-direction (in the opposite side of the closer free edge to the concentrated load)
$V_{control}$	total shear force going through the evaluated direction along the slab width
V_{Ed}	design shear action
$V_{Ed,red}$	design shear action reduced by the factor related to arching action β_{shear}
V_{Fu}	shear force due to the concentrated load F_u
$V_{R,net}$	net value of the one-way shear capacity
V_{test}	measured one-way shear force at failure in the tests for a section at $a/2$.
V_R	one-way shear capacity
$V_{R,predicted}$	predicted one-way shear resistance
$V_{Rd,CEN,}$	design shear resistance according to the NEN 1992-1-1:2005 [17]
P_{test}	maximum applied concentrated load at failure
P_{Rd}	design punching capacities
$P_{predicted}$	predicted punching resistance
F_{flex}	concentrated load associated with the slab flexural capacity according to the yield line analysis
$P_{R,punching}$	total shear force resisted by punching
$\beta_{arching}$	factor related to arching action
$\beta_{torsion}$	parameter that considers the relative effect of torsion on the capacity of the strips
γ	concrete specific weight (assumed = 24 kN/m^3 in this study)
γ_c	partial safety factor of concrete
ψ_{ij}	slab rotation in each side of the control perimeter
$\varepsilon_{y,L}$	is the flexural reinforcement yield strain of the longitudinal rebars
$\varepsilon_{y,T}$	is the flexural reinforcement yield strain of the transverse rebars
ρ_{avg}	average flexural reinforcement ratio considering both directions
ρ_l	flexural reinforcement ratios in longitudinal direction
ρ_t	flexural reinforcement ratio in transverse direction
σ_{cp}	average normal concrete stress over the cross-section, positive in compression
AVG	average

COV	coefficient of variation
P	observed failure mode is punching failure
SS	test was performed with the load closer to the simple support
LVDT	linear variable differential transformers
WB	observed failure mode is wide beam shear failure
WB + P	the observed failure mode combines characteristics of WB and P
WB + P + Y	the observed failure mode combines characteristics of WB, P and extensive reinforcement yielding on failure

occurs. Therefore, it is important to evaluate shear and punching capacity predictions for members with reinforcement yielding.

In the case of concentric punching tests, some authors [11,12] already pointed out that a brittle punching failure could occur after limited reinforcement yielding, and they identified this type of failure as flexure-induced punching. For such cases, the ultimate load would be lower than the predicted punching capacity and also lower than the flexural capacity predicted by yield line analyses $F_{yieldline}$. Although the flexural capacity predicted by yield line analysis constitutes an upper-bound solution, large deviations were not expected for simple boundary conditions (concentric tests). For instance, Hawkins and Ospina [15] pointed out that in some tests rated as critical in flexure (predicted flexural capacity lower than the predicted punching capacity), the reinforcement started to yield at the load of 50 % of $F_{yieldline}$, and flexure-induced punching occurred at 80 % of $F_{yieldline}$. While flexure-induced punching is studied and well-understood for two-way slabs [11,12,15], limited information is available for one-way slabs under concentrated loads with reinforcement yielding [16].

This study investigates the ultimate capacity and failure mechanism of one-way slabs under concentrated loads subjected to local flexural reinforcement yielding at failure. As such, this paper tries to answer the research question of how local reinforcement yielding influences the failure mechanism and ultimate capacity of one-way slabs under concentrated loads. First (Section 2), this study tries to provide a broader look into the problem by evaluating three possible failure mechanisms: one-way shear as wide beams, punching shear around the load and flexural failure. Section 3 describes the performed experiments to investigate the problem more closely. The ultimate loads, cracking pattern, load–deflection response and reinforcement strains monitored during the tests allowed to identify the influence of the local reinforcement yielding at the failure (Section 4). In Section 5, the test results are discussed in more detail according to the parameters varied between similar tests (parameter analyses): (i) load position and (ii) span length. At the end (Section 6), a comparison between tested and expected resistances was performed to discuss how the local reinforcement yielding influenced the predictions of shear, punching and flexural capacity of the slabs.

2. Code provisions for one-way, two-way shear and flexural capacity

2.1. Design code expressions for one-way shear

In most design codes, the sectional shear capacity V_R (or one-way shear capacity) of slabs is determined by multiplying the nominal shear capacity (shear force capacity per unit area, $v_{R,shear}$) by a given length, usually called effective shear width b_{eff}, and by the effective depth to the longitudinal reinforcement d_l. The sectional shear capacity $V_{Rd,EC,}$ according to the current European code NEN EN 1992-1-1:2005 [17], can be calculated as:

$$V_{Rd,CEN} = v_{Rd,CEN} \cdot b_{eff} \cdot d_l$$

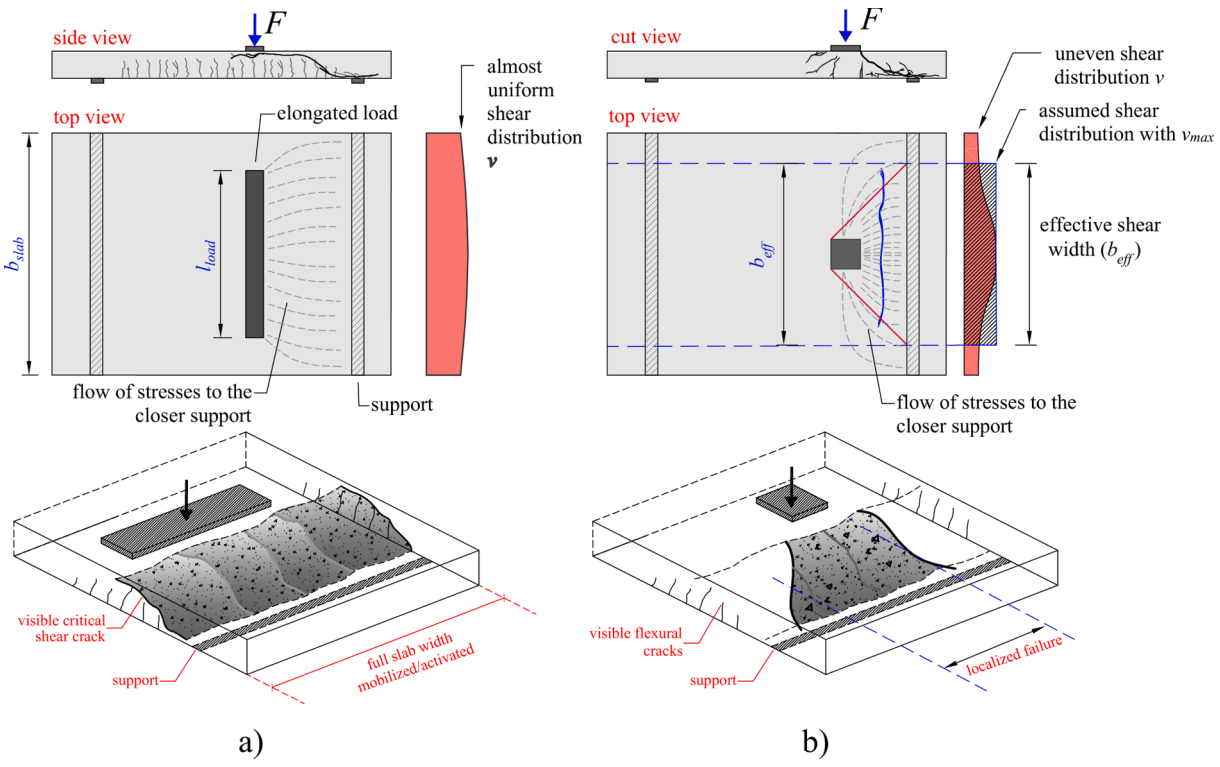

Fig. 1. (a) Sketch of a slab failing as a wide beam in one-way shear with a critical shear crack visible at the slab side due to the reduced ratio b_{slab}/l_{load} and (b) slab failing by a combination of punching and one-way shear along a limited slab strip due to the larger ratio b_{slab}/l_{load}.

$$v_{Rd,CEN} = \max\begin{Bmatrix} [C_{Rd,c}k_{CEN}(100\rho_l f_{ck})^{1/3} + k_1\sigma_{cp}] \\ (v_{\min} + k_1\sigma_{cp}) \end{Bmatrix} \quad (2)$$

With f_{ck} in [MPa], b_{eff} in [m], d_l in [mm] and $k_1 = 0.15$ for NEN EN 1992-1-1:2005.

$$v_{\min} = 0.035k_{CEN}^{3/2}f_{ck}^{1/2} \quad (3)$$

$C_{Rd,c}$ is an empirical factor used for characteristic shear strength calculations, and it was derived from comparison with experimental results [18] and calibrated through reliability analysis on 176 beam tests [19]. In the NEN EN 1992-1-1:2005 is used the value of $C_{Rd,c} = 0.18/\gamma_c$. For comparisons between tested and predicted resistances, the term $C_{Rd,c}$ was replaced in this study by $C_{R,c,test} = 0.15$, as suggested by Lantsoght et al. [20].

$$k_{CEN} = 1 + \sqrt{\frac{200}{d_l}} \leqslant 2, \text{ with } d_l \text{ in [mm]} \quad (4)$$

In the next sections, the comparisons between tested and predicted resistances are performed by replacing characteristic values such as f_{ck} by measured ones as f_{cm}. Besides, all partial factors γ are assumed as 1. In this way, V_{Rd} becomes $V_{R,predicted}$.

The effective shear width b_{eff} herein was determined based on the French guidelines [21,22], which assumes the load spreading from the back faces of the loading plate towards the support with 45-degree angles (Fig. 1b). According to this approach, the effective shear width increases as the shear slenderness a_v/d_l increases. This choice was motivated based on previous investigations that showed the best accuracy of this approach for loads close to the support [23,24].

The NEN EN1992-1-1:2005 [17] accounts for the influence of direct load transfer depending on the clear shear span to effective depth ratio a_v/d_l. According to this code, the contribution of a load applied within a distance $0.5\,d_l < a_v < 2\,d_l$ from the edge of the support to the shear force caused by the concentrated load (V_{Fu}) may be multiplied by the reduction factor $\beta_{arching}$:

$$\beta_{arching} = \frac{a_v}{2d_l} \begin{cases} \geqslant 0.25 \\ \leqslant 1.00 \end{cases} \quad (5)$$

Consequently, the determination of the reduced shear demand ($V_{E,red}$) that should be compared to the one-way shear resistance $V_{R,predicted}$ assumes the following expression:

$$V_{E,red} = V_{Fu}\cdot\beta_{arching} + (v_g + v_{fq})\cdot b_{slab} \quad (6)$$

where v_g is the shear force per unit meter caused by the self-weight and v_{fq} is the shear force caused by line loads or other axles of loads on the control section (not applied in this study).

According to some authors [25,26], direct load transfer could be considered an enhancement to the sectional shear capacity $V_{R,predicted}$ equivalent to the decrease of the shear demand. Therefore, we included $\beta_{arching}$ in the determination of the shear capacity $V_{R,predicted}$ by multiplying the calculated nominal shear capacity v_R for $1/\beta_{arching}$. In this way, V_E and $V_{R,predicted}$ become:

$$V_E = V_{Fu} + v_g\cdot b_{slab} \quad (7)$$

$$V_{R,predicted} = \left(v_R\cdot\frac{1}{\beta_{arching}}\right)\cdot b_{eff}\cdot d_l \quad (8)$$

2.2. Design code expressions for two-way shear or punching

The punching capacity P_R is commonly determined as the product of the nominal punching capacity (shear stress, $v_{R,punch}$), the calculated resisting control perimeter b_0 and effective depth d_{avg}. Therefore, the punching shear capacity for NEN EN 1992-1-1:2005 [17] can be calculated as:

$$P_{Rd} = v_{Rd,punch}\cdot(b_o\cdot d_{avg}); \quad (9)$$

$$v_{Rd,punch} = \max\begin{Bmatrix} [C_{Rd,c}k_{CEN}(100\rho_{avg}f_{ck})^{1/3}] \\ (v_{\min} + k_1\sigma_{cp}) \end{Bmatrix} \quad (10)$$

With d_{avg} in [mm] and f_{ck} in [MPa]

$$\rho_{avg} = (\rho_l\cdot\rho_t)^{1/2} \quad (11)$$

$$v_{\min} = 0.035k_{CEN}^{3/2}f_{ck}^{1/2} \quad (12)$$

$$k_{CEN} = 1 + \sqrt{\frac{200}{d_{avg}}} \leqslant 2, \text{ with } d_{avg} \text{ in [mm]} \quad (13)$$

For comparisons between tested and predicted resistances (next sections), the following changes are applied: (i) f_{ck} is replaced by f_{cm} in the expressions; (ii) partial safety factors are taken equal 1; (iii) $C_{R,m,p} = 0.18$. In this way, $v_{Rd,punch}$ becomes $v_{R,punch}$. The shear-resisting control perimeter is set at $2d_{avg}$ from the load edges (Fig. 2a). In the case of loads closer to the support, however, the intersection of the control perimeter with the support shall be considered (Fig. 2b).

In the calculations of the punching capacity, the self-weight should also be considered in determining the effective punching capacity. In this case, it is assumed that the self-weight acts only in the span direction and, hence, it decreases only the net shear resistance of the sides $b_{0,x1}$ and $b_{0x,2}$ of the shear resisting control perimeter (see Fig. 3).

$$\begin{aligned} v_{R,punch,net,1} &= v_{R,punch} - v_{sw,1} \\ v_{R,punch,net,2} &= v_{R,punch} - v_{sw,2} \end{aligned} \quad (14)$$

Despite not being discussed in most design codes, we also considered the influence of arching action in the punching capacity predictions, as first suggested by Regan [27]. In this way, we used the same factor considered for one-way shear $\beta_{arching}$ in the portion of the control perimeter closer to the support ($b_{0,x1}$). Therefore, the punching capacity is calculated considering the uneven distribution of the shear resistance over the control perimeter by the following expression:

$$P_{R,predicted} = \left[v_{R,punch,net,1}\cdot\frac{1}{\beta_{arching}}\cdot b_{0,x1} + v_{R,punch,net,2}\cdot b_{0,x2} + v_{R,punch}\cdot(b_{0,y1} + b_{0,y2})\right]\cdot d_{avg} \quad (15)$$

2.3. Predictions of ultimate capacity with yield lines

The load capacity was also calculated based on yield line analysis, which provides the load capacity based on the flexural mechanism F_{flex}. Three configurations of yield line were considered as studied by Belletti et al. [13] (Fig. 4).

The following expressions were applied to calculate the load capacity for each mechanism.

Mechanism 1:

$$F_{flex,mech1} = \left(m_{sag,x}\cdot\frac{b_{slab}}{a}\right) + \left(m_{sag,x}\cdot\frac{b_{slab}}{b}\right) + 2\cdot\left[m_{sag,y}\cdot\frac{(a+b)}{0.5\cdot b_{slab}}\right] - l_{span}\cdot b_{slab}\cdot\gamma_{conc}\cdot\frac{h_{slab}}{3} \quad (16)$$

Mechanism 2:

$$F_{flex,mech2} = \left(m_{sag,x}\cdot\frac{b_{slab}}{b}\right) + 2\cdot\left(m_{sag,y}\cdot\frac{a}{0.5\cdot b_{slab}}\right) + 2\cdot\left(m_{sag,y}\cdot\frac{b}{0.5\cdot b_{slab}}\right) - (a\cdot b_{slab}\cdot\gamma_{conc}\cdot h_{slab}\cdot 0.5 + b\cdot b_{slab}\cdot\gamma_{conc}\cdot h_{slab}\cdot 1/3) \quad (17)$$

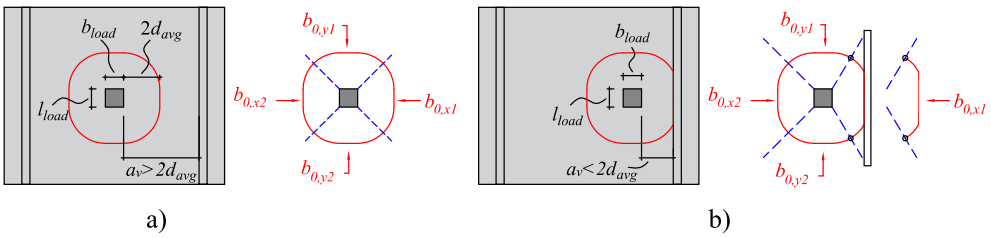

Fig. 2. Control perimeter and partition of the control perimeter for loads (a) placed at $a_v > 2d_{avg}$ and (b) loads placed at $a_v < 2d_{avg}$.

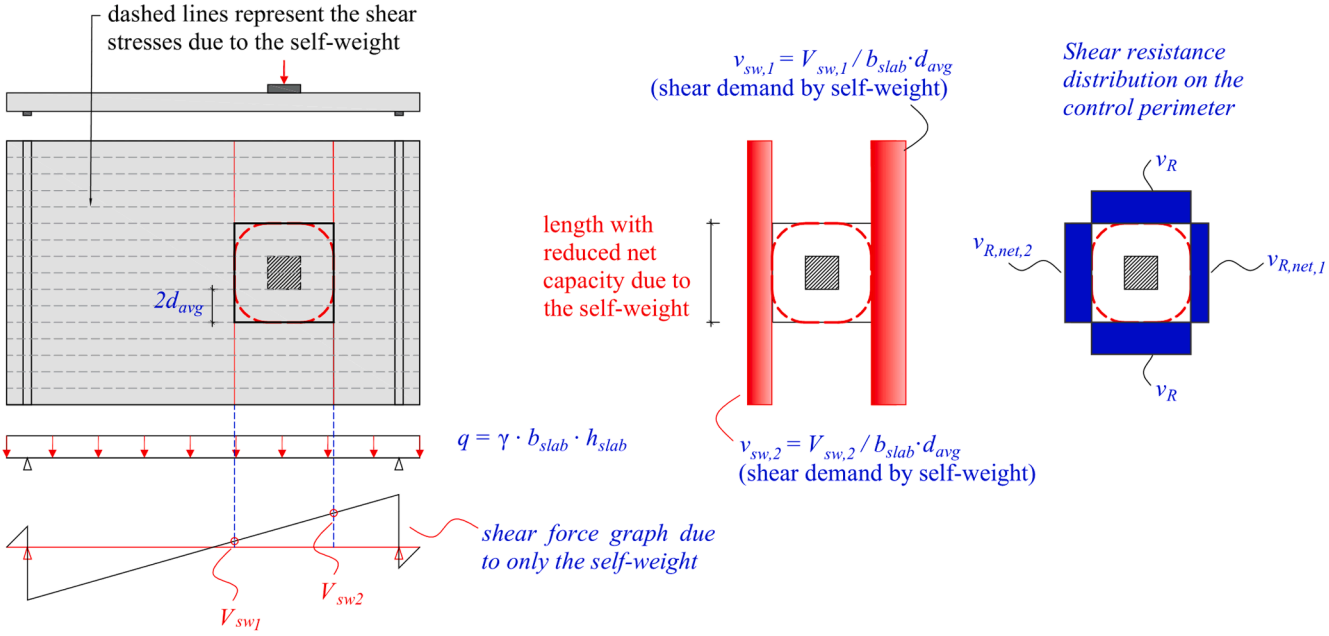

Fig. 3. Distribution of the shear demand due to the self-weight in the shear resisting control perimeter and determination of the distribution of the shear resistance around the load. Note: a square control perimeter was used by simplification to illustrate this effect.

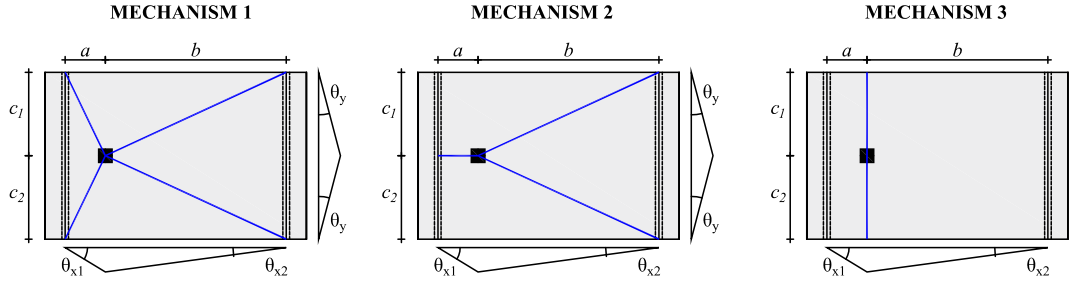

Fig. 4. Yield line mechanisms for simply supported slabs under CL based on Belletti et al. [13].

Mechanism 3:

$$F_{flex,mech3} = m_{sag,x} \cdot \frac{b_{slab}}{a} + m_{sag,x} \cdot \frac{b_{slab}}{b} - l_{span} \cdot b_{slab} \cdot \gamma_{conc} \cdot h_{slab} \cdot 0.5 \quad (18)$$

At this point, the reader shall realize that collapse mechanism 3 would provide similar results to that using sectional analyses with the concentrated load F resulting in $M_R = M_E$, with M_R and M_E being the flexural resistance and acting bending moment in the longitudinal direction, respectively, assuming the one-way slab as a beam loaded over the entire width. Minor differences in the results can be attributed to the assumed position of the internal level arm z in the section analyses.

Using elastic finite element analyses (FEA), the concentrated load to cause a flexural failure is generally defined as the lower one between that which causes $m_{E,x} = m_{sag,x}$ and $m_{E,y} = m_{sag,y}$ (m_E and m_{sag} are the acting unitary bending moment and unitary flexural capacity in the evaluated direction, respectively). In general, such approaches may provide overly conservative predictions since it does not consider the capacity of redistribution of inner forces when $m_R = m_E$ at a certain point. Because of this, in design, it's usual to calculate an average bending moment over a certain length that varies between 2 d_l and 4 d_l around the peak or, often used in bridge engineering, over 3 m (notional lane width). In this study, the predictions using yield line analyses were used instead of FEA to keep the employed methods of evaluation within the scope of analytical calculations and also based on the good acceptance of such methods combined with punching capacity calculation models [28].

2.4. Determination of the most critical failure mechanism comparing one-way shear and two-way shear capacity predictions

In this study, we compared the tested and predicted resistances to determine which would be the most critical failure mechanism theoretically. In order to compare which would be the most critical failure mechanism in a clear way, we compared the predicted ultimate loads F that would cause a one-way shear failure ($F_{predicted,shear}$), a punching shear failure ($F_{predicted,punching}$), and a flexure failure (F_{flex}) predicted by yield line analyses.

To determine the concentrated load $F_{predicted,shear}$ associated with the predicted sectional shear capacity $V_{R,predicted}$, the influence of the self-weight was considered in the following way. First, the net value of the shear capacity $V_{R,net}$ that should resist only the concentrated load was calculated since part of the shear capacity is used to resist the self-weight v_g.

$$V_{R,net} = V_{R,predicted} - v_g \cdot b_{slab} \tag{19}$$

Next, the relation between the applied load and the respective shear force ($F \leftrightarrow V_{Fu}$) caused by the concentrated load was used (fixed value which depends only on the statics of the problem) to determine the applied load $F_{predicted,shear}$ corresponding to the sectional shear capacity $V_{R,net}$.

$$F_{predicted,shear} = V_{R,net} \cdot \frac{F_{test}}{V_{Fu,test}} \tag{20}$$

In the case of the punching capacity predictions, the term $F_{R,predicted,punching}$ is equal to $P_{R,predicted}$, calculated with the punching expressions and considering the influence of the self-weight (expression (15)). Alternatively, we could also calculate the total punching load P_{test} (summing the applied concentrated load F_{test} and the portion of the shear demand due to the self-weight transferred by the control perimeter). In these cases, the comparisons could be performed in terms of P_{test}/P_R.

Comparing the relations $V_{test}/V_{R,predicted}$ with $F_{test}/F_{R,predicted,shear}$ for the studied slabs from Section 3, the differences were commonly lower than 2 % due to the limited value of v_g compared to v_R for the scaled slabs tested in the laboratory. The same level of differences occurred for the punching predictions. Therefore, one can also directly compare the relations $V_{test}/V_{R,predicted}$ with $F_{test}/F_{predicted,punching}$ and with F_{test}/F_{flex} to determine the most critical failure mechanism between one-way shear, punching shear and flexure. Comparing the ratios $F_{test}/F_{predicted,shear}$, $F_{test}/F_{predicted,punching}$, F_{test}/F_{flex}, one can observe that the higher value determines the most conservative prediction and the theoretically most critical failure mechanism.

2.5. Predictions with the Extended Strip Model

The Extended Strip Model (ESM) is a plasticity-based model that describes a lower-bound solution to the load capacity of slabs under concentrated loads [29]. This model is based on the bond model developed for concentric punching shear [30](Fig. 5a), which combines the two-way flexure within the quadrants and arching action from one-way shear in the strips. Failure occurs when the unitary shear capacity w_{ACI} at the interfaces of the strips and quadrants is reached. As the unitary shear capacity w_{ACI} is based on expressions that assume reinforcement yielding at failure, the ESM indirectly considers reinforcement yielding and possible load redistribution at ultimate states, similar to the yield line mechanisms. Fig. 5b shows the assumed pattern of strips and quadrants for a general case, on which the load is placed eccentrically in the longitudinal and transverse directions of the slab.

The total load capacity in the ESM is given by P_{ESM}:

$$P_{ESM} = P_x + P_{sup} + P_y + P_{edge} \tag{21}$$

$$P_x = \sqrt{2 \cdot (1 + \beta_{torsion}) \cdot M_{sag,x} \cdot w_{ACI,x}} \tag{22}$$

$$P_{sup} = \frac{2 \cdot d_l}{a_v} \cdot \sqrt{2 \cdot (1 + \beta_{torsion}) \cdot M_{s,x} \cdot w_{ACI,x}} \tag{23}$$

$$P_y = \sqrt{2 \cdot \left(\frac{L}{L - a_M}\right) \cdot M_{s,y} \cdot (w_{ACI,y} - v_{DL})} \tag{24}$$

$$P_{edge} = \begin{cases} \sqrt{2 \cdot \beta_{torsion} \cdot \left(\frac{L}{L - a_M}\right) \cdot M_{s,y} \cdot (w_{ACI,y} - v_{DL})} & \text{for } l_w < l_{edge} \\ \sqrt{\beta_{torsion} \cdot \left(\frac{L}{L - a_M}\right) \cdot (w_{ACI,y} - v_{DL}) \cdot l_{edge}} & \text{for } l_w \geq l_{edge} \end{cases} \tag{25}$$

P_{sup}, P_x, P_y and P_{edge} are the capacities of the four strips around the load for simply supported or continuous slabs. P_{sup} is the capacity of the strip between the closer support and the load in the longitudinal direction; P_x is the capacity of the strip between the load and the far support in the longitudinal direction. P_y and P_{edge} are the capacities of the strips in the transverse direction (considering the load placed eccentrically along the

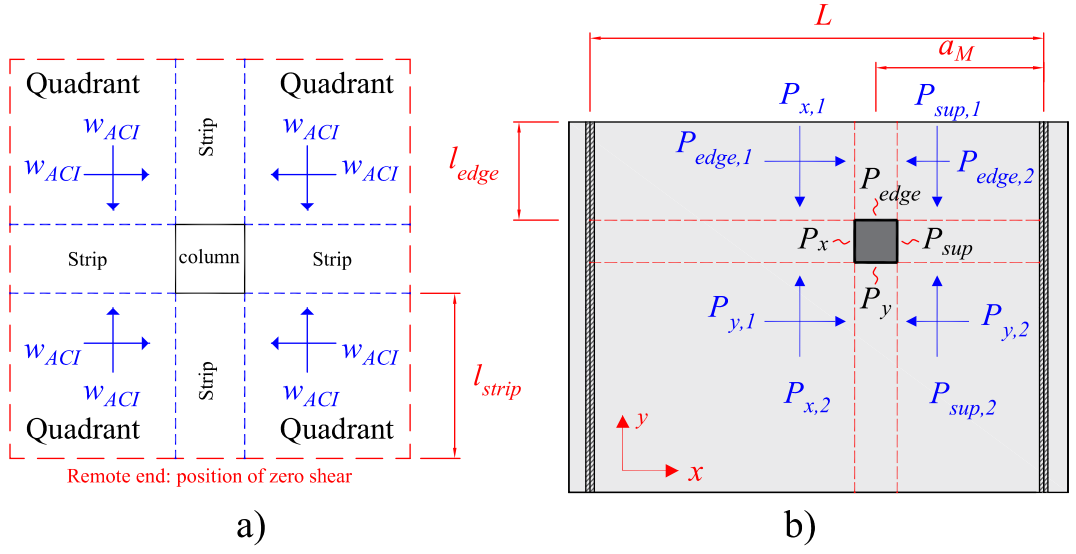

Fig. 5. (a) Layout of the original bond model with strips and quadrants; (b) Layout of the strips and quadrants for the Extended Strip Model in simply supported slabs (Adapted from [29]).

slab width). When the concentrated load is placed at the center of the slab width, P_{edge} is calculated as P_y, and no torsion is considered in the transverse direction. Therefore, the following expression can be applied:

$$P_{ESM} = P_x + P_{sup} + 2P_y \tag{26}$$

$\beta_{torsion}$ is the parameter that considers the relative effect of torsion on the capacity of the strips:

$$\beta_{torsion} = 0.8 \cdot \frac{a}{d_x} \cdot \frac{b_r}{b_{slab}}, \text{ for } 0 \leqslant \frac{a}{d_x} \leqslant 2.5 \text{ and } 0 \leqslant \frac{b_r}{b_{slab}} \leqslant \frac{1}{2} \tag{27}$$

l_{edge} is the distance between the free edge and the edge of the concentrated loads in the slab width direction; b_r is the distance between the slab free edge and the load axis. The loaded length of the strip l_w is a reference parameter for loads close to the free edge of one-way slabs and is calculated as:

$$l_w = \sqrt{\frac{2 \cdot M_{s,y}}{\beta_{torsion} \cdot (w_{ACI,y} - v_{DL}) \cdot \frac{L}{L - a_M}}} \tag{28}$$

L is the span length between two supports for simply supported slabs and the largest distance between the farthest support (from the load) and the point of contraflexure for loads close to continuous support. a_M is the center-to-center distance between load and support (simply supported slabs) or between load and point of contraflexure (continuous members), whichever is smaller. v_{DL} is the unitary shear demand due to the dead load over the strips in the y-direction. The following expressions were applied to compute $M_{sag,x}$ and $M_{sag,y}$:

$$M_{sag,x} = \rho_{x,bottom} \cdot f_{y,x,bottom} \cdot l_{load} \cdot d_{x,bottom}^2 \cdot \left(1 - \frac{f_{y,x,bottom} \cdot \rho_{x,bottom}}{1.7 \cdot f_{cm}}\right) \tag{29}$$

$$M_{sag,y} = \rho_{y,bottom} \cdot f_{y,y,bottom} \cdot b_{load} \cdot d_{y,bottom}^2 \cdot \left(1 - \frac{f_{y,y,bottom} \cdot \rho_{y,bottom}}{1.7 \cdot f_{cm}}\right) \tag{30}$$

$w_{ACI,x}$ and $w_{ACI,y}$ are the unitary capacities (shear force per unit length) calculated according to the ACI 318–14 [31] and corrected by a size effect factor as:

$$w_{ACI,x} = 0.167 \cdot d_{y,bottom} \cdot \sqrt{f_{cm}} \cdot \left(\frac{100}{d_{y,bottom}}\right)^{1//3} \tag{31}$$

$$w_{ACI,y} = 0.167 \cdot d_{x,bottom} \cdot \sqrt{f_{cm}} \cdot \left(\frac{100}{d_{x,bottom}}\right)^{1/3} \tag{32}$$

3. Experimental investigation

3.1. Test setup

This study focuses on one-way slabs with a small thickness (150 mm) compared to previous investigations [1,2,6,8,10]. The tested slabs had relatively high longitudinal reinforcement ratios (ρ_l = 0.99 % and ρ_l = 1.32 %). The specimens represent short-span bridges from rural roads typically found in Brazil. Besides, this thickness can also be representative of certain floor slabs found in industrial plants, nuclear buildings [32] or building slabs loaded with heavy equipment during construction or use [3]. In Brazil, a large number of rural bridges and river culverts in reinforced concrete are built to facilitate the grain flow on farms and rural roads [33]. These bridges and culverts have span lengths that can be very limited (2 m − 6 m), and the slab thickness varies between 150 mm and 250 mm. Nowadays, many timber bridges are being replaced by reinforced concrete slabs (sometimes prefabricated) and reinforced concrete box culverts, as illustrated in Fig. 6.

Fig. 7 shows a sketch of the test setup. In total, six slabs were tested at the São Carlos School of Engineering (EESC) from the University of São Paulo, and each slab was tested twice. The specimens measured 3.40 m × 1.60 m × 0.15 m (h_{slab} = 150 mm). The line supports (Support 1 and Support 2 in Fig. 7a) consisted of a 100 mm wide steel hinge, a rubber layer of 10 mm and two instrumented aluminum beams. The rubber layer was used between the slab bottom face and the steel-hinged supports (Fig. 9a). The measured rubber layer stiffness is approximately 110 MPa (110 N mm/mm^3) (Fig. 9b) based on a direct compression test on samples of 100 mm × 100 mm × 10 mm. The hinged supports rested on instrumented aluminum beams to estimate the distribution of reaction forces, inspired by the work of Natário et al. [8]. Fig. 9 shows a detail of the supports.

In the first test of each slab, the span length between the supports was 3 m (Fig. 7a). After conducting the first test close to support 1, a second test was conducted close to support 2 (Fig. 7b). the span length was reduced in the second test to 2 m, as performed in other experimental studies [6,37] to remove the influence of failure caused by the first test. Fig. 8 shows some pictures of the test setup.

The concentrated load was applied in a displacement-controlled manner through a 400 kN servo-controlled actuator. The loading was applied onto a 200 mm × 200 mm × 30 mm square plate. The size of the load was chosen in such a way as to provide a relation between the slab width and load size in the transverse direction b_{slab}/l_{load} = 8. In a previous study, this value for the ratio b_{slab}/l_{load} was identified as a possible point of transition from governing one-way shear failure to punching failures [38]. Hence, both the one-way shear and punching shear failures could be critical for such slabs. Besides, this load size is similar to that used in other publications [1,39,40], which could facilitate the comparison between test results.

The load positions tested were a_v/d_l = 1, a_v/d_l = 2 and a_v/d_l = 3, with, a_v the clear shear span (measured between the inner edges of the loading plate and support), and d_l the effective depth of the longitudinal reinforcement (span direction). These values were chosen to study the failure mechanism of the slabs (shear, punching or flexure) when direct load transfer could play a significant role in the tests.

a) b) c)

Fig. 6. Example of rural bridges commonly found in Brazil: (a) prefabricated two-way slabs for a composite bridge [34] (b) culvert bridge [35] and (c) prefabricated deck slab [36].

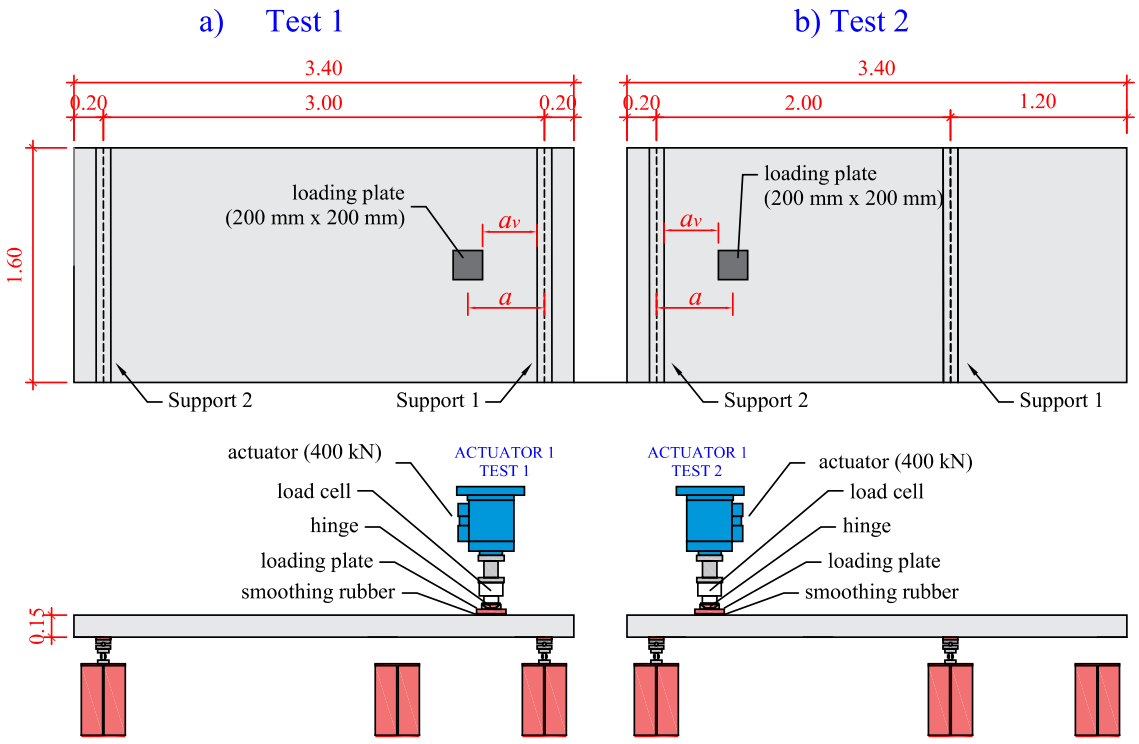

Fig. 7. Sketch of test setup used in the experimental program for each slab: (a) test 1 and (b) test 2.

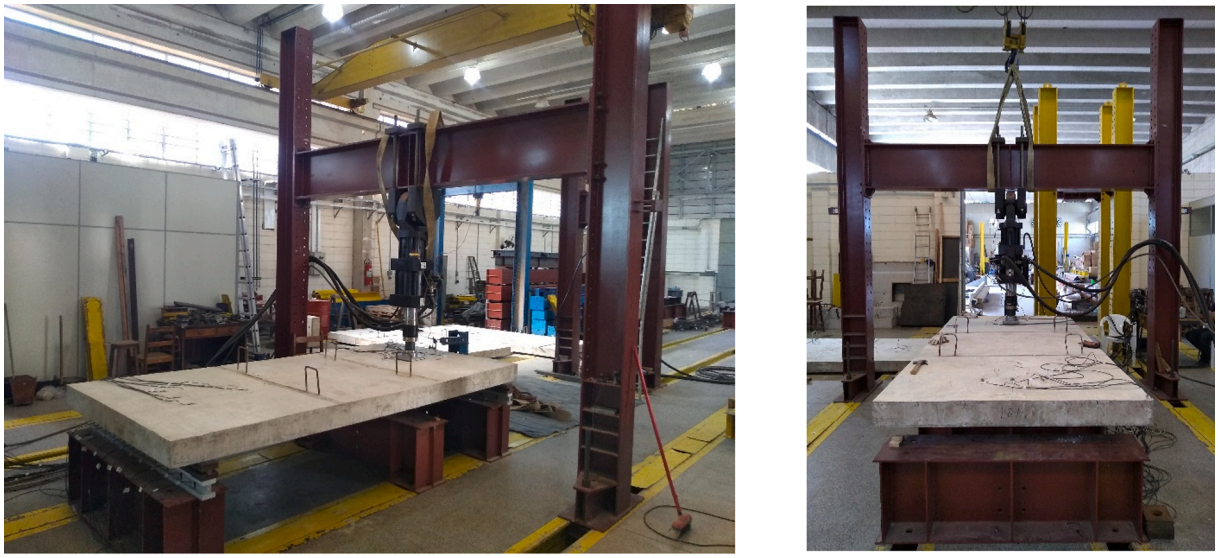

Fig. 8. Pictures of the test setup: (a) view in perspective (position of test 1); (b) view of the backside (position of test 2).

3.2. Specimens

The experimental program consisted of six slabs of 3.4 m × 1.60 m × 0.15 m. The slab properties are given in Table 1. The letter "N" or "S" indicates the first or the second test (N = first test and S = second test). Two mixes of concrete were used for the slabs. The concrete compressive strength ($f_{c,cyl}$) was measured at cylinder specimens of 100 mm × 200 mm. The concrete tensile strength ($f_{ct,sp}$) was determined with splitting tests on cylinder specimens with 100 mm × 200 mm. The maximum aggregate size was 19.0 mm for both mixes. Basaltic coarse aggregates were used.

The slabs L1, L2 and L3 were tested at ages 51 days, 52 days and 53 days after pouring. The slabs L4, L5 and L5 were tested at ages of 28 days, 29 days and 30 days after pouring. No significant difference in the concrete compressive strength was verified in the experiments from the same mix with differences of 1 or 2 days of age. Because of this, the results are reported as an average of the measured values for each mix. Fig. 10 shows the measured stress–strain behavior in compression for both concrete mixes used. Both mixes develop a large post-peak regime.

The longitudinal reinforcement ratios were chosen to study the combination of reinforcement yielding with shear and punching failures. The bottom longitudinal reinforcement of the slabs consisted of

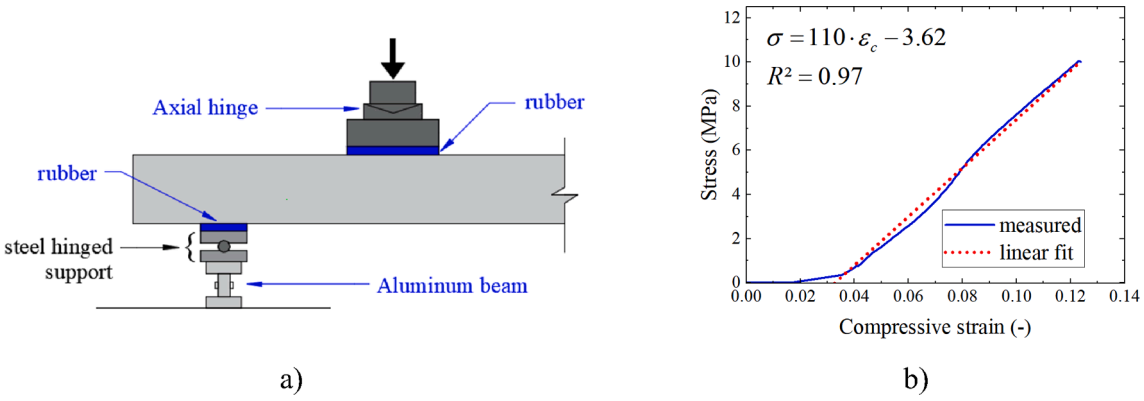

Fig. 9. (a) Assembly of the support (rubber layer, hinged support and aluminum beam; (b) calculation of the average elastic stiffness of the rubber.

Table 1
Main properties of slabs L1 to L6. Note: the number between parentheses represents the coefficient of variation.

Ref-Test	$f_{c,cyl}$ (MPa)	$f_{ct,sp}$ (MPa)	ρ_l (%)	ρ_t (%)	a_v/d_l [-]	a/d_l [-]	l_{span} (m)
L1-N	22.0	2.36	0.99	0.44	1.00	2.21	3
L1-S	(12.0 %)	(11.0 %)			1.00	2.21	2
L2-N					2.00	3.21	3
L2-S					2.00	3.21	2
L3-N					3.00	4.21	3
L3-S					3.00	4.21	2
L4-N	28.3	2.63	1.32	0.44	1.00	2.21	3
L4-S	(10.6 %)	(12.6 %)			1.00	2.21	2
L5-N					2.00	3.21	3
L5-S					2.00	3.21	2
L6-N					3.00	4.21	3
L6-S					3.00	4.21	2

12.5 mm bars at 100 mm ($\rho_l = 0.99$ %) or 12.5 mm bars at 75 mm ($\rho_l = 1.32$ %). The effective depth of the main longitudinal and transverse reinforcement is $d_l = 123.8$ mm and $d_t = 113.5$ mm, respectively. The bottom reinforcement in the transverse direction of the slabs consisted of 8 mm bars at 100 mm, resulting in $\rho_t = 0.44$ %. The top reinforcement in the longitudinal and transverse directions (compression reinforcement) consisted of 8 mm diameter bars at 200 mm ($\rho_{l,comp} = 0.20$ % and $\rho_{t,comp} = 0.21$ %). The reinforcement layout of the two series of slabs is shown in Fig. 11.

The properties of the deformed bars were measured by performing direct tensile tests on rebar samples. The measured properties of the 12.5 mm diameter bars are: $f_{ym} = 514$ MPa; $E_s = 205$ GPa. The deformed bars with a diameter of 8 mm have the following properties: $f_{ym} = 513$ MPa and $E_s = 197$ GPa.

3.3. Instrumentation

During the tests, the following parameters were measured: applied load *F*, vertical displacements of the slab, strains at the tensile reinforcement, and strain distribution along the support beam (aluminum beam). The actuator system directly measured the applied load *F*. The vertical displacements of the slab were measured by linear variable differential transformers (LVDTs). LVDT (1) and LVDT (2) were applied for the vertical slab deflections. The main vertical displacements monitored were at the center of the slab and at the distance of $d_l/2$ from the loading plate face. The arrangement of the sensors is shown in Fig. 12.

Strains at the longitudinal and transverse reinforcement were also monitored by a couple of strain gauges glued to the rebar in each direction. The position of the strain gauges was always within the square of the loading plate, as sketched in the next sections.

4. Experimental results

4.1. Ultimate load and load–displacement curves

Few studies have investigated the failure mechanism of one-way slabs under concentrated loads with local reinforcement yielding [16]. In this study, all tests presented some degree of reinforcement-yielding at failure or presented a shear failure at the onset of reinforcement-yielding (as shown in more detail in the next sections). Table 2 describes the peak loads (F_{test}) applied in the tests and the tested shear

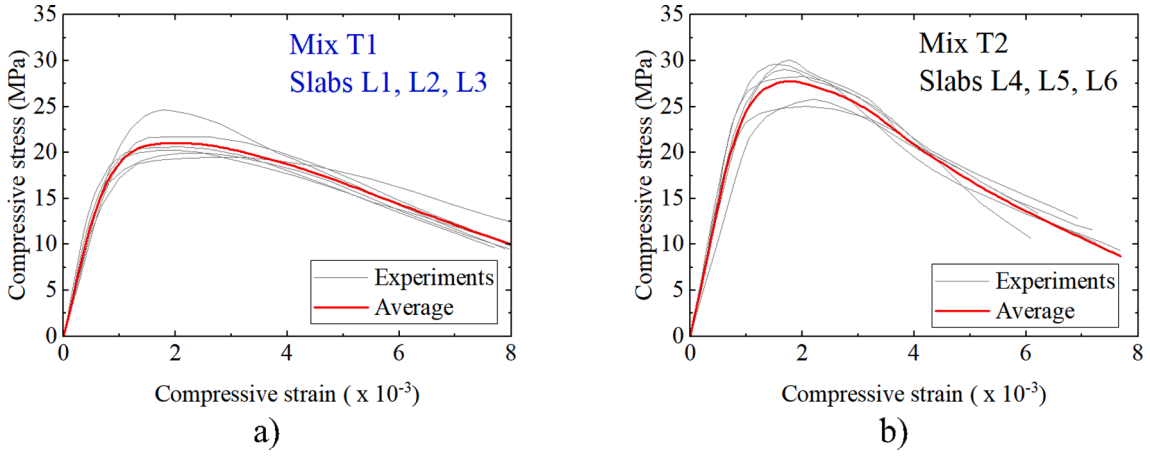

Fig. 10. Compression stress–strain behavior of the tested concrete mixes: (a) 22 MPa mix and (b) 28 MPa mix.

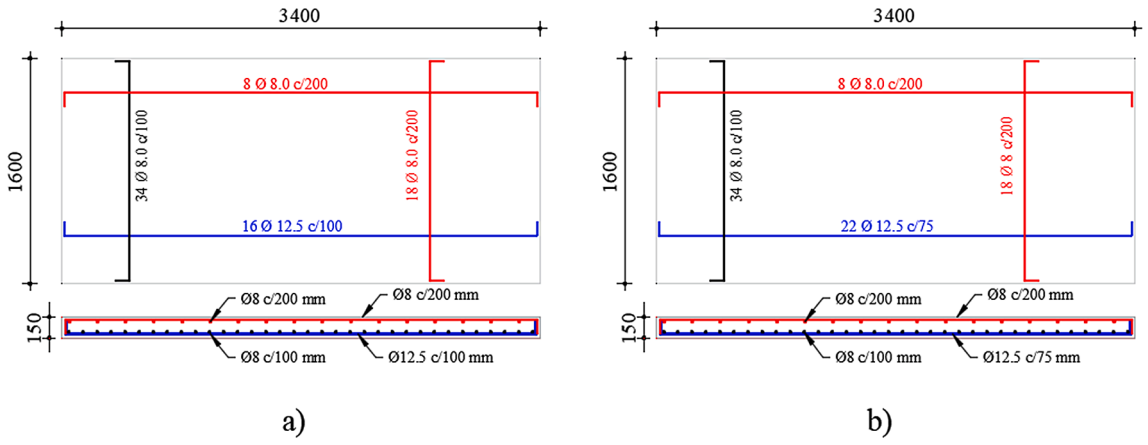

Fig. 11. Geometry and reinforcement layout of the slabs (a) L1, L2 and L3; (b) L4, L5 and L6. All dimensions in mm.

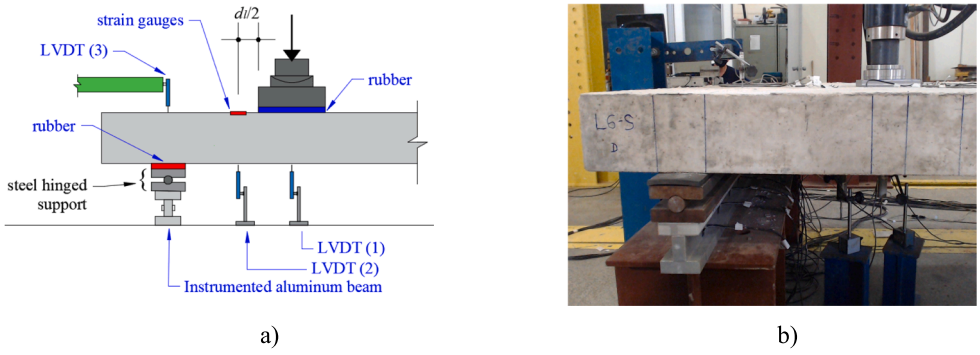

Fig. 12. Sketch of the instrumentation: a) side view showing the position of sensors; b) side picture of the test L6-S.

Table 2
Tested loads and failure mode for slabs L1 to L6.

Test	l_{span} (m)	f_{cm} (MPa)	f_{ctm} (MPa)	ρ_l (%)	ρ_t (%)	a_v/d_l (-)	a/d (-)	Failure mode	F_{test} (kN)	V_{test} (kN)
L1-N	3	22.0	2.36	0.99	0.44	1	2.21	WB + P	273.5	256.4
L2-N	3	22.0	2.36	0.99	0.44	2	3.21	WB + P + Y	282.1	252.3
L3-N	3	22.0	2.36	0.99	0.44	3	4.21	WB + P + Y	275.4	234.7
L4-N	3	28.3	2.63	1.32	0.44	1	2.21	WB + P	351.5	327.3
L5-N	3	28.3	2.63	1.32	0.44	2	3.21	WB + P	321.6	286.5
L6-N	3	28.3	2.63	1.32	0.44	3	4.21	WB + P + Y	267.0	227.8
L1-S	2	22.0	2.36	0.99	0.44	1	2.21	WB + P	332.1	291.6
L2-S	2	22.0	2.36	0.99	0.44	2	3.21	WB + P	270.4	221.3
L3-S	2	22.0	2.36	0.99	0.44	3	4.21	WB + P	253.9	192.0
L4-S	2	28.3	2.63	1.32	0.44	1	2.21	P	374.1	327.9
L5-S	2	28.3	2.63	1.32	0.44	2	3.21	WB + P + Y	296.3	242.0
L6-S	2	28.3	2.63	1.32	0.44	3	4.21	P	314.8	237.0

Notes: WB = wide beam shear failure (one-way shear, including both shear-compression and flexure-shear failures); P = punching; Y = combination of extensive reinforcement yielding at failure and ductile failure based on the graph $F \times \delta$.

capacity (V_{test}), assuming the static scheme of a beam. The self-weight was considered in V_{test} by assuming $\gamma_{self} = 25$ kN/m^3 and the shear force V_{test} was calculated at the mid-shear span between the center of the load and the center of the support as a simplification since the position of the critical shear crack varies between the load and support according to the loading position [41,42]. Table 2 also describes the main material properties, failure mechanism and load layout for each test. As the failure mechanism classification was based on different observations from the test results (cracking pattern, measured strains at the reinforcement and load – deflection graphs); this failure mode identification is detailed in the next sections.

Fig. 13 shows the load–displacement (F–δ) graphs measured by LVDT (1) for each specimen tested: a) tests L1-N to L3-N; b) tests L1-S to L3-S; c) tests L4-N to L5-N and d) tests L4-S to L6-S. In Fig. 13, the LVDT(1) results were corrected by the support displacements (see Fig. 12) to provide the net slab deflection.

All specimens presented a higher displacement at the peak load as the shear slenderness a_v/d_l increased (for instance, comparing the test results from L1-N to L3-N or from L4-N to L6-N). The only exception occurred for the pair of tests L4-S ($a_v/d_l = 1$) and L5-S ($a_v/d_l = 2$), which developed almost the same deflection at the peak load. Even though they reached similar deflections at failure, L4-S developed a relatively stiffer behavior in the load–displacement graph than L5-S, as expected. By comparing the deflections at the peak load for tests having the same reinforcement ratio and shear slenderness but with a lower span length, it can be seen that the displacements at the peak load decreased as the

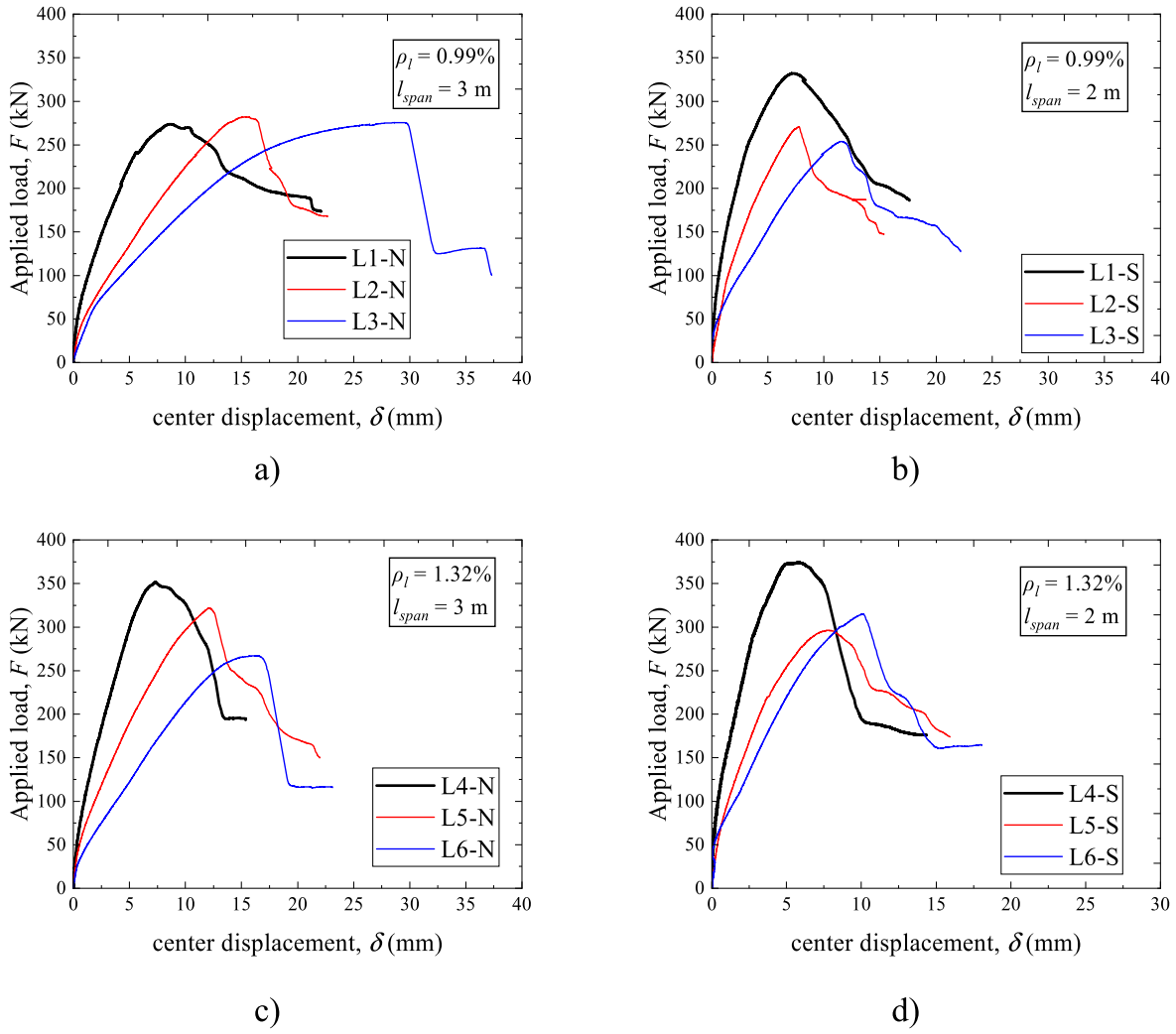

Fig. 13. Load–displacement (F–δ) graphs for: (a) tests L1-N to L3-N; (b) L1-S to L3-S; (c) L4-N to L5-N and (d) L4-S to L6-S. Note: the displacements measured by LVDT(1) below the concentrated load were corrected by the displacements measured at the support.

span length decreased, also consistent with flexural theory.

By evaluating the shape of the load–deflection curves around the peak load (Fig. 13), typical brittle shear failures (L5-N and L6-N, for instance) and shear failures with a limited amount of post-peak ductility (test L1-N, for instance) were observed. At the peak load, all tests developed a partial punching cone towards the closest support (as shown in the next sections). After this, and after increasing the applied displacement at the loading plate, a large redistribution of shear forces took place. In some tests, a second failure mechanism developed: wide beam shear failure (WB) with the shear crack visible at the slab sides (Fig. 16 and Fig. 17).

4.2. Reinforcement strains

The shear force redistribution of one-way slabs decreases the brittleness at failure [8,43,44]. This phenomenon has been investigated more based on the redistribution of shear forces at the support [6,8,44,45]. In this study, the evolution of the strain on the instrumented rebars also confirms this phenomenon. Fig. 14 and Fig. 15 show the distribution of the strains at the longitudinal (L1 and L2) and transverse (T1 and T2) reinforcement with the applied load (F).

For instance, Fig. 14a shows that after reaching the peak load, the longitudinal reinforcement strains stop increasing, even though the applied displacement of the actuator increases. On the other hand, the transverse reinforcement strain increases as the applied displacement increases. Monitoring the reinforcement strain confirms that after a local punching failure, the transverse reinforcement allows the redistribution of internal stresses around the load. On the other hand, after the development of the punching cracks on the front side of the load, the longitudinal reinforcement seems to reach a plateau of strains.

The comparison between Fig. 14a, Fig. 14b and Fig. 14c (increasing the shear span from L1-N to L3-N) demonstrates that the relation between the measured strains at the longitudinal reinforcement with the strains at the transverse reinforcement increases substantially.

These strains can identify another phenomenon. The measured reinforcement strains on the two instrumented longitudinal rebars matched closely for most tests, and this is the expected behavior due to the tests' intended symmetric geometric. In practice, some minor deviations of the loading frame or of the reinforcement position could occur during the assembly (<5 mm) or during the concrete casting, resulting in small imperfections. This aspect explains deviations in the measured strains at the longitudinal rebars from small load levels (for instance, L2-2). However, it is noteworthy that even for the tests where a close match of measured strains was possible at the beginning of the tests ($F < 0.5\ F_{max}$ for L2-N, L3-N, L3-S), the deviations in the reinforcement strains at some point increase due to the asymmetrical cracking pattern of concrete structures. In practice, this occurs due to the unequal and randomly distributed tensile strength of the concrete, which causes a crack to arise at the weakest point first.

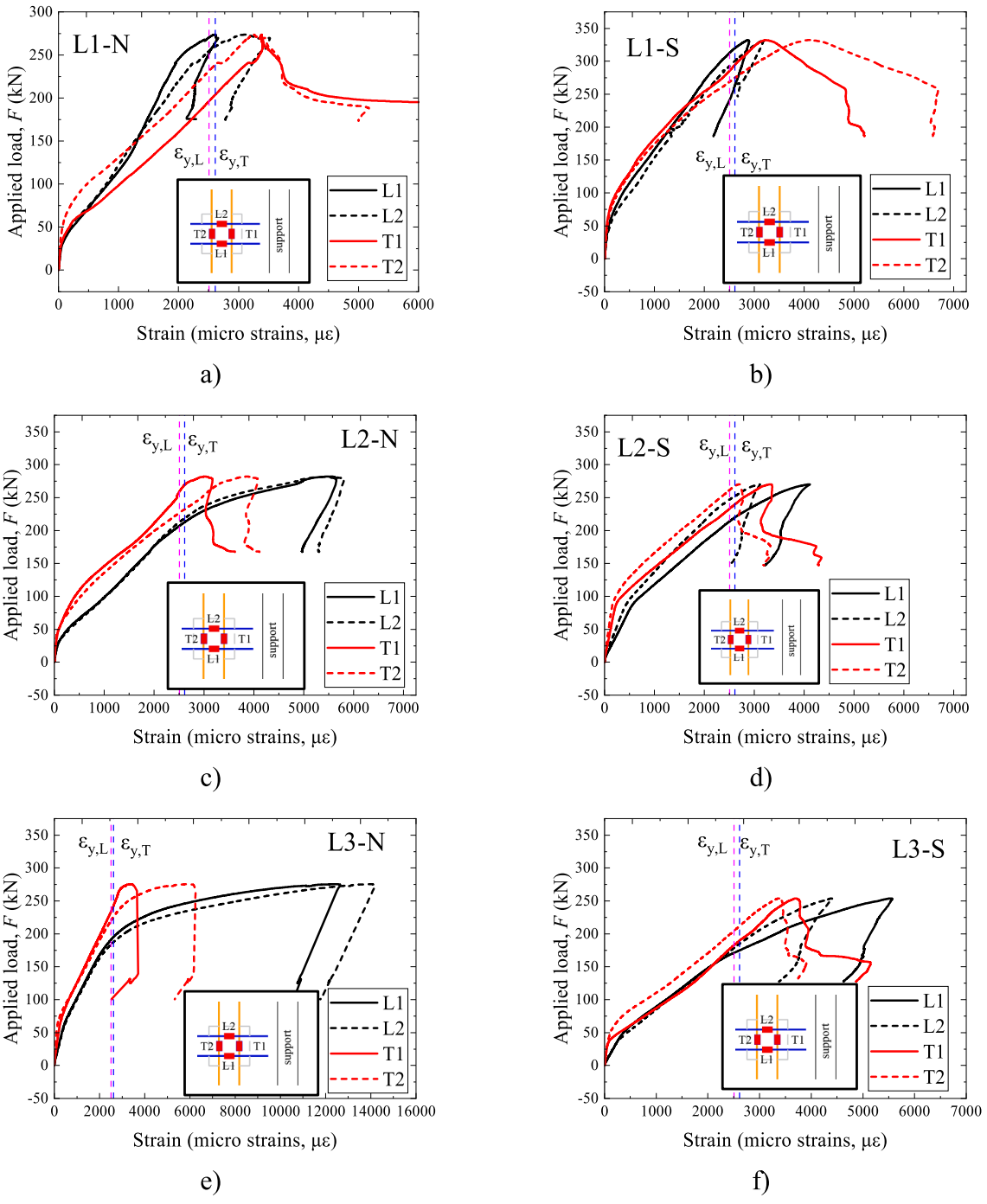

Fig. 14. Evolution of reinforcement strains around the loaded area during the tests: (a) test L1-N; (b) test L1-S; (c) test L2-N; (d) test L2-S; (e) test L3-N; (f) test L3-S. Note: $\varepsilon_{y,L}$ is the yielding strain of the longitudinal reinforcement and $\varepsilon_{y,T}$ is the yielding strain of the transverse reinforcement.

4.3. Cracking pattern

The cracking pattern is one of the best parameters to indicate the failure mechanisms that took place in the slabs. Fig. 16 and Fig. 17 show the cracking pattern of the slabs around the loaded area for each test. Cracks in the top view, bottom view and side views were tracked mainly after unloading of the slabs. Different from shear and punching shear cracks, some flexural cracks closed after unloading and are not visible at the time of crack marking (for instance, side views of L6-S in Fig. 17).

The following criteria were used to determine the shear failure mechanism based on the cracking pattern:

- Punching: cracks are commonly visible at the compression side of the slab because inclined cracks from punching commonly reach the load edges. Due to the asymmetrical position along the shear span, an asymmetrical punching cone would be expected for such slabs. Tangential and circumferential cracks are also visible at the tension side of the slabs
- One-way shear: inclined cracks visible at the slab side would indicate that one-way shear took place as the governing failure mechanism (if punching crack are not visible at the compression side of the slab) or after shear redistribution (after a first punching failure).

The top view of the slabs shows that all tests presented an

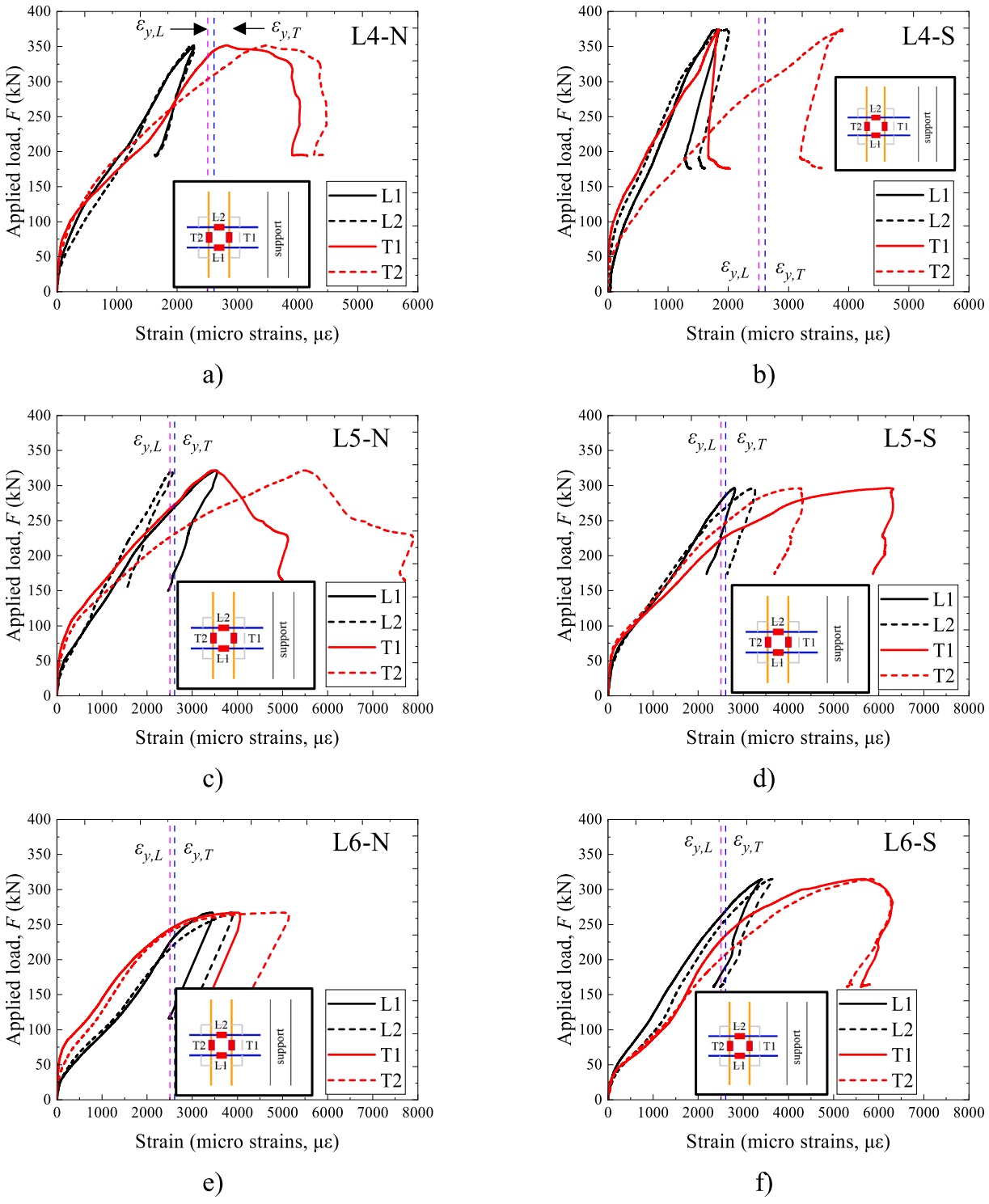

Fig. 15. Evolution of reinforcement strains around the loaded area during the tests: (a) test L4-N; (b) test L4-S; (c) test L5-N; (d) test L5-S; (e) test L6-N; (f) test L6-S. Note: $\varepsilon_{y,L}$ is the yielding strain of the longitudinal reinforcement and $\varepsilon_{y,T}$ is the yielding strain of the transverse reinforcement.

asymmetrical punching failure starting between the front sides load and support (as detailed in Fig. 18a for the test L1-S). The bottom view of the slabs L1-N, L2-N and L3-N shows a large presence of tangential and circumferential cracks around the load, as expected for punching failures (Fig. 16). Slabs L4-N, L5-N and L6-N presented fewer visible cracks due to the higher reinforcement ratio in the longitudinal direction, which decreased the crack width at failure (Fig. 17). Fig. 18b shows an example of the cracking pattern at the bottom side for the test L3-N (red lines indicate visible cracks after testing).

In most tests, concrete detachment close to the support was visible (see an example of L1-N in Fig. 18c), which helps to explain why most publications considered the most critical section for one-way shear analyses for simply supported slabs at the face of the support. Nowadays, with the aid of finite element models [2], the idea that the section near the load is governing is more common, which explains the punching failures visible in the top and bottom views. The side views of the tests show that, after a first punching failure, many tests experienced a large redistribution of forces around the load. This behavior occurs due to the

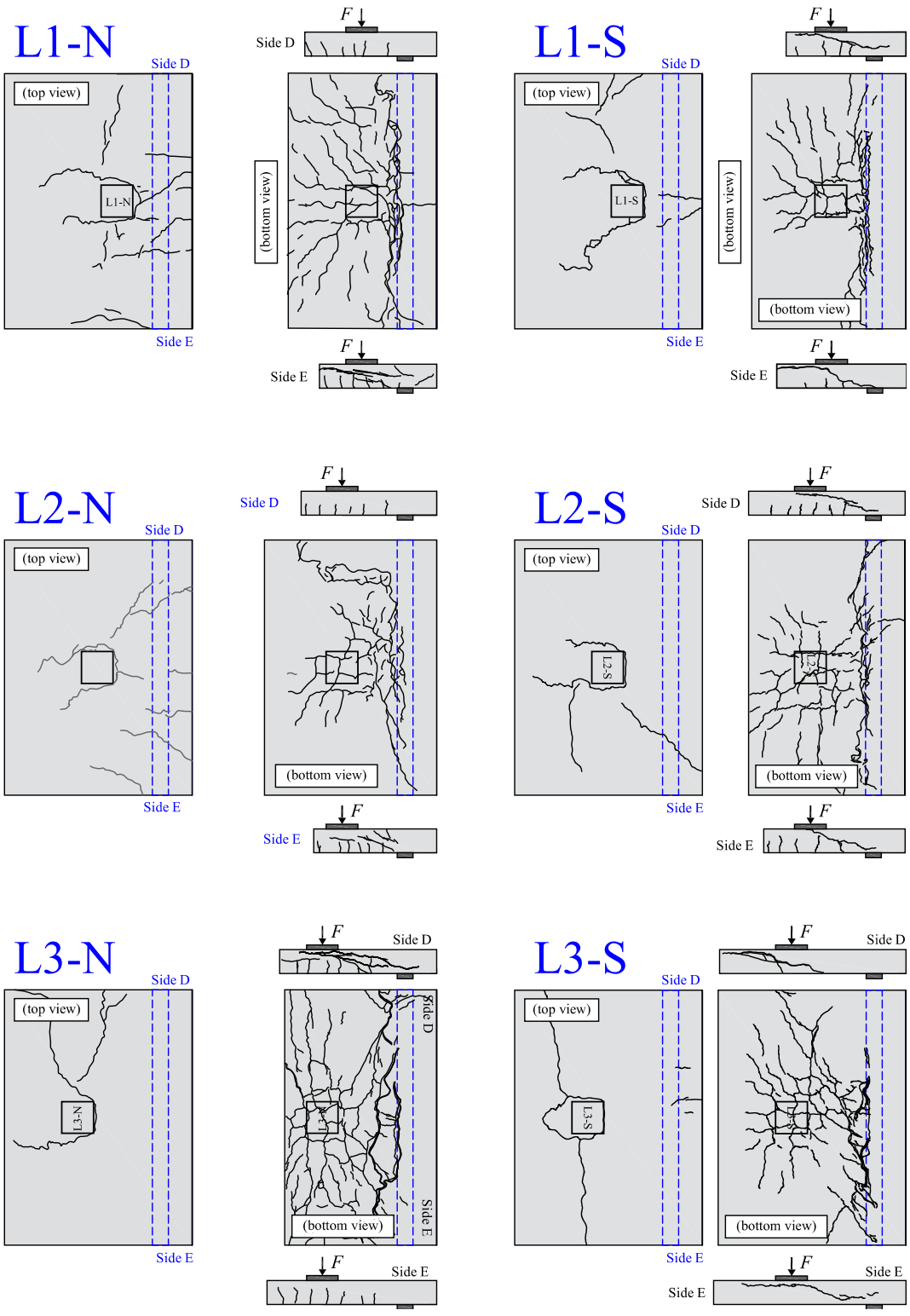

Fig. 16. Cracking pattern of the slabs L1, L2 and L3 in terms of top view, bottom view and side views.

relatively high transverse reinforcement ratio applied for the tested one-way slabs ($\rho_t = 0.44$ %). Fig. 18d shows an example of such cracks for the test L2-S).

Fig. 19 shows a summary of the cracking pattern visible at the side of the slabs after tests. The red lines indicate the position of a virtual strut between the load and the support, which aid to identify if shear-compression failures took place in the tests. At this point, the following criteria were used to determine the one-way shear failure mode at the slab sides:

- Shear-compression: tests with inclined cracks inside the virtual strut indicate shear-compression failures. For such tests, the cracking pattern generally does not indicate reinforcement detachment at the tensile side (horizontal cracks at the reinforcement level possibly caused by dowel action) and the main cracks reach the load edge with steeper inclinations.

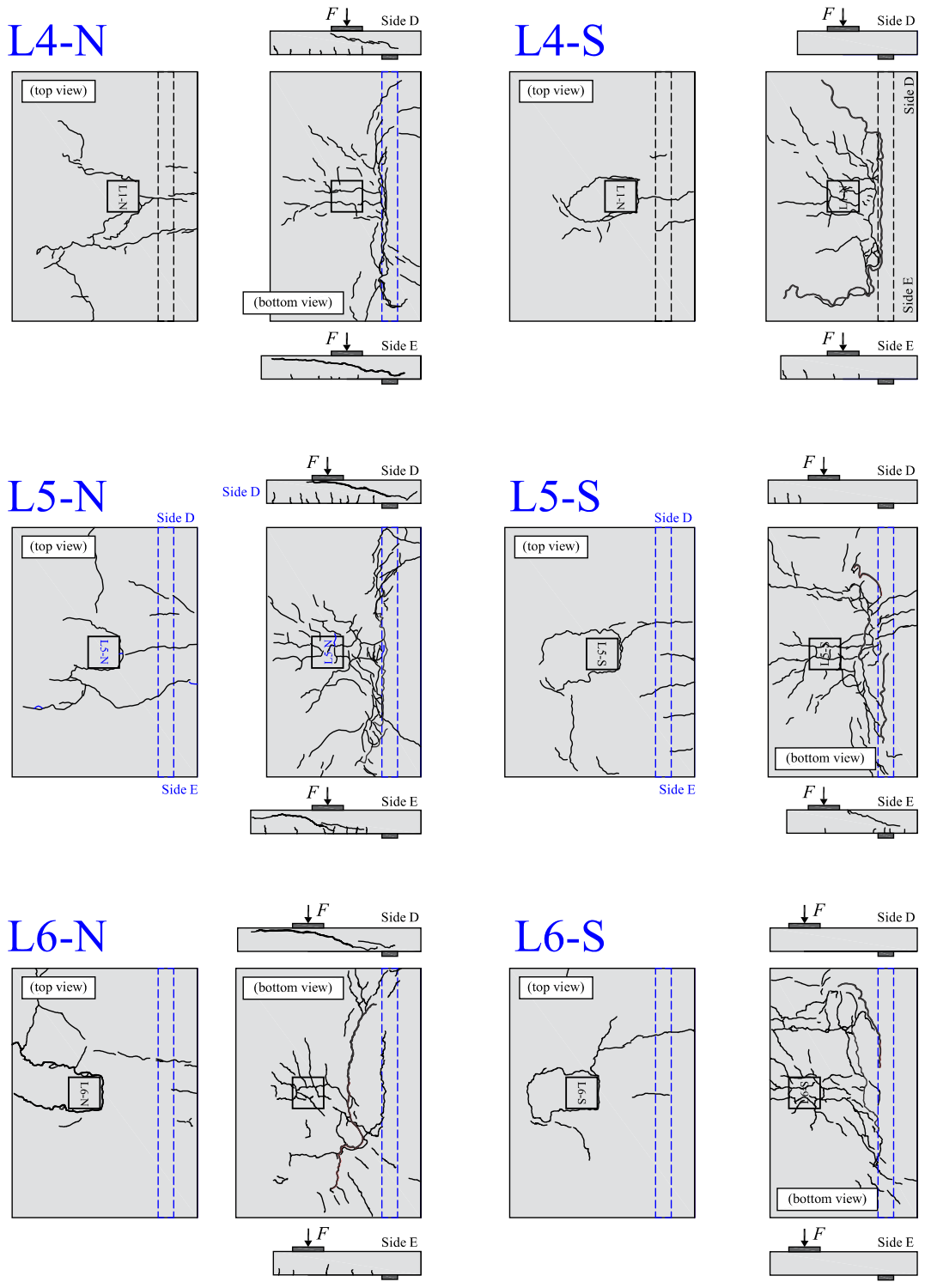

Fig. 17. Cracking pattern of the slabs L4, L5 and L6 in terms of top view, bottom view and side views.

- Flexure-shear: cracks with a curved shape indicate flexure-shear failures. Besides, the cracking pattern of flexure-shear commonly shows almost horizontal cracks close to the tensile reinforcement and in the compression zone, and an inclined crack between them in the shear span, resulting in a typical "S-shaped" crack.

The tests L1-N (side E), L2-N (side E) and L3-N (side D) developed a visible shear crack on one of the sides (Fig. 19e,f), but the inclination of the cracks indicates failure in the strut zone by shear-compression (steeper cracks not following the flexural cracks). Since these tests were performed with the load close to the support, such failures could be expected due to the large contribution of direct load transfer between the load and the support.

The Test L1-S presented characteristics from both shear-compression (side D) and flexure-shear failures (side E). The test L2-S was classified as failing by shear-compression because of the position of the inclined crack. On the other hand, the test L3-S present more characteristics from flexure-shear failures (horizontal cracks in the compression side and at

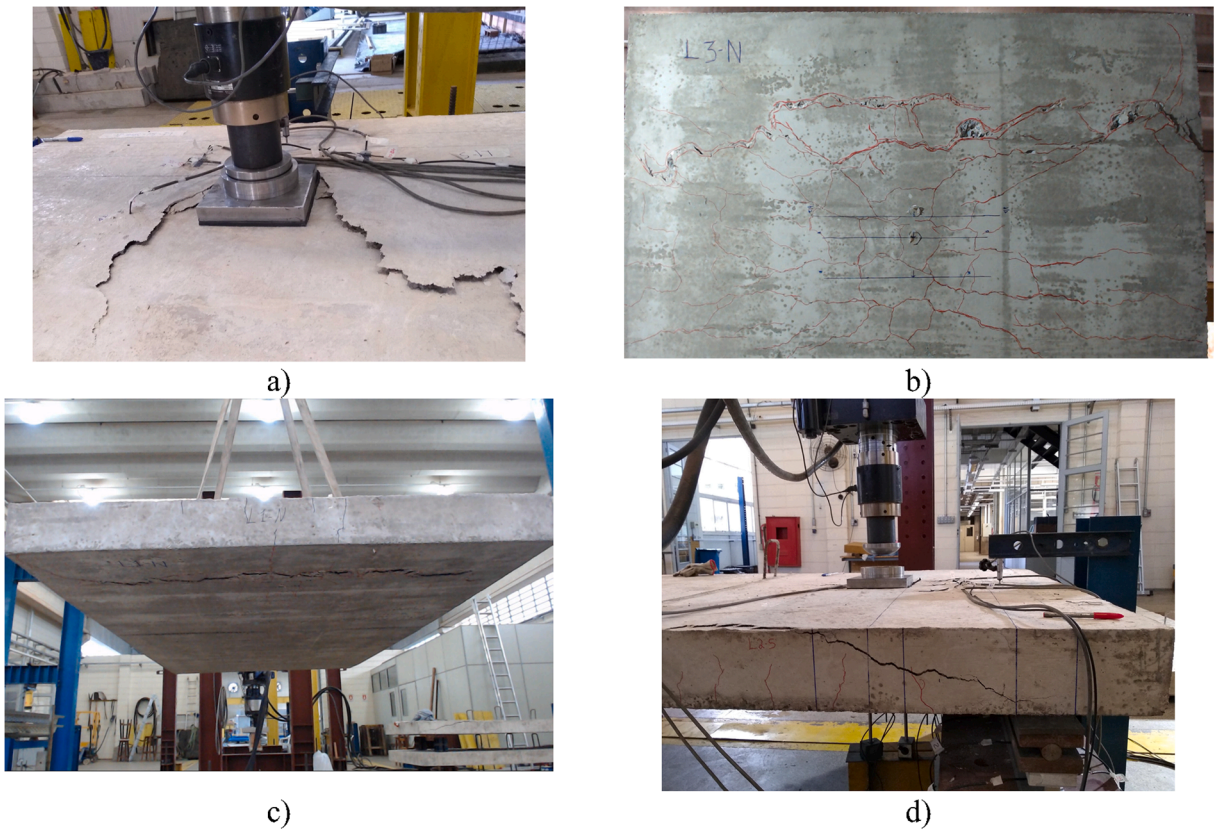

Fig. 18. Details of the cracking pattern of the slabs: (a) punching cracks at the top side of the slabs (P); (b) cracking at the bottom side of the slab L3-N; (c) detail of the crack opening close to the support for L1-N; (d) example of shear cracks from wide beams (WB) visible at the slab sides of the test L2-S.

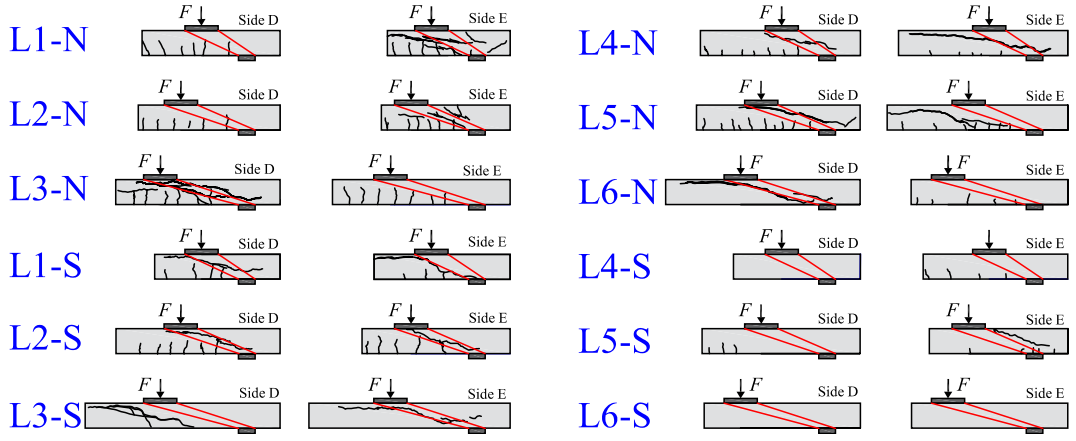

Fig. 19. Cracking pattern at the side of the tested slabs.

the reinforcement level), despite the inclined crack situated within the virtual strut in Side E.

The visible cracking pattern of the test L4-N is subjected to discussion. Side D indicates a shear-compression failure, while side E could be a large inclined crack from flexure-shear or only the result of a wide punching failure. The test L5-N shows a shear-compression failure at Side E and a flexure-shear failure at the side D. The shape of the cracking pattern from L6-N indicates a flexure-shear failure: some horizontal cracks at the reinforcement level and others crossing the compression zone.

The test L4-S did not present visible cracks at the slab sides, indicating a pure punching failure around the load. On the other hand, the test L5-S shows a shear-compression crack on one side. The test L6-S did not show visible shear cracks at the slab sides.

4.4. Failure mechanism overview

Table 3 shows a summary of the major characteristics considered in the classification of the failure mechanism. The failure mechanism was determined based on three aspects: (i) the shape of the force–displacement curve measured by the LVDT (1); (ii) the tensile strains from the instrumented rebars around the load; and (iii) the cracking pattern.

In most tests, the strain gauges indicated some reinforcement yielding at the peak load F_{test}. However, to be classified as clear yielding that is expected with the yield line analyses, a plateau would be necessary in the load–displacement curves (such as commonly found in

Table 3
Main aspects considered in the determination of the governing failure mechanism of the slabs.

Test	Sharp decrease of the applied load on failure?	Extensive yielding of all rebars at F_{max}?	Punching cone at the top view?	Shear crack visible at the slab sides?	Indication of shear-compression?	Failure mode
L1-N	No	No	Yes	Yes: one side	Yes	WB + P
L2-N	No	Yes	Yes	Yes: one side	Yes	WB + P + Y
L3-N	No	Yes	Yes	Yes: one side	Yes	WB + P + Y
L1-S	Yes	No	Yes	Yes: two sides	Yes (one side)	WB + P
L2-S	Yes	No	Yes	Yes: two sides	Yes	WB + P
L3-S	Yes	Yes	Yes	Yes: two sides	Yes/No	WB + P
L4-N	No	No	Yes	Yes: two sides	No	WB + P
L5-N	Yes	No	Yes	Yes: two sides	Yes/no	WB + P
L6-N	No	Yes	Yes	Yes: one side	Not clear	WB + P + Y
L4-S	No	No	Yes	No	Not visible	P
L5-S	No	Yes	Yes	Yes: one side	Yes (one side)	WB + P + Y
L6-S	Yes	Yes	Yes	No	No visible	P

tests of beams, where a large increase in displacements until reaching crushing of the concrete and the flexural failure occurs after yielding of the steel). Because of this, no test was classified as failing by flexure, although some of them presented large reinforcement yielding at failure (tests L3-N and L6-N) or a smooth decrease in the applied load prior to failure (tests L1-N, L4-N, L4-S and L5-S). However, we identified the tests on which extensive strains at the reinforcement and a short plateau in the load–deflection graphs arose, since these could indicate a started flexural mechanism (letter Y in the failure mode classification).

5. Influence of parameters

5.1. Effect of the shear slenderness a_v/d_l

The shear slenderness a_v/d_l is a parameter in the literature commonly related to the identification of tests subjected to possible arching action [1,10,23]. Such a mechanism increases the ultimate loads at failure when a_v/d_l descreases due to the direct load transfer between the load and the support, which appears as an additional shear-transfer mechanism in addition to the beam shear-transfer mechanisms: (i) aggregate interlock; (ii) compression zone capacity; (iii) dowel action and (iv) residual tensile strength of the concrete. The Eurocode [17] and *fib* Model Code 2010 [46] consider arching action in the range $0 \leq a_v/d_l \leq 2$. Other publications suggest extending the range of influence until $a_v/d_l = 2.5$ [20] and $a_v/d_l = 2.75$ [8]. As performed in previous publications [1], the predicted one-way shear resistance enhancement was calculated based on the $\beta_{arching}$ factor from EN-1992-1-1:2005 [17] (Section 2.1 and expression (8)). The predicted concentrated loads $F_{predicted,shear}$ to cause a one-way shear failure was calculated as in Section 2.4 (expression (20). The predicted concentrated load to cause a punching failure $F_{predicted,punching}$ was calculated as in Sections 2.2 and 2.4.

Fig. 20 shows how the peak loads and sectional shear forces vary as the shear slenderness a_v/d_l changes for the four sets of tests. As can be seen in Fig. 20a, the ultimate loads (F_{test}) did not change significantly (<6 %) by increasing the shear slenderness from $a_v/d_l = 2$ to $a_v/d_l = 3$ for most tests. The only exception was the set of tests L4-N to L6-N, which presented a decrease of the load F_{test} of 17 % (comparing L5-N and L6-N). The tested sectional shear V_{test} decreased between 2 % (L5S to L6-S) and 20 % (L5-N to L6-N). According to the factor $\beta_{arching}$ used, no change of the nominal shear capacity $v_{R,shear}$ was expected in the range $2 \leq a_v/d_l \leq 3$. However, the effective French shear width increases by 23 %, increasing the ratio a_v/d_l from 2 to 3. In the end, the predicted concentrated loads to cause a one-way shear failure ($F_{predicted,shear}$) would increase between 29 % and 33 %, varying a_v/d_l from 2 to 3 (note that such enhancement is not 23 % because the proportion between F and V_{Fu} also changes as a function of a_v/d_l). Consequently, an enhancement of F_{test} would be expected for all tests using one-way shear expressions, which was not observed. These results occur because increasing the

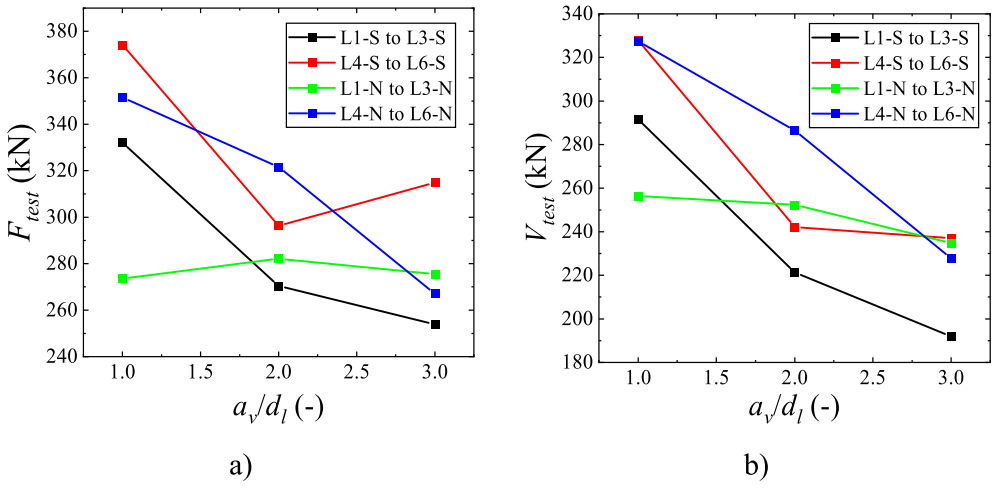

Fig. 20. Influence of shear slenderness a_v/d_l or distance from the concentrated load to support: (a) on tested peak loads F_{test} and (b) on calculated shear forces V_{test}.

shear slenderness a_v/d_l increases the bending moments around the load and, hence, decreases the unitary shear capacity v_R according to the Critical Shear Crack Theory (CSCT) models for one-way shear [47] and two-way shear [28]. In this way, possible enhancements in the effective shear width are counterbalanced by reductions of the shear capacity. On the other hand, using the punching shear expressions, no enhancement of the punching capacity ($F_{predicted,punching}$) would be expected in this range of a_v/d_l (changes lower than < 1 %). Therefore, the predictions of punching capacity better match the tested loads and also the failure mechanism, which starts with punching for all slabs.

On the other hand, the ultimate load F_{test} increased considerably as the shear slenderness a_v/d_l decreased from 2 to 1 for most groups of tests. This increment was 19 % between L1-S and L2-S, 9 % between L4-N and L5-N, and 21 % between L4-S and L5-S. The only exception occurred for the set of tests L1-N and L2-N, which presented almost the same peak loads at failure. Using the one-way shear expressions, the predicted enhancement in the concentrated loads $F_{test,predicted,shear}$ varied between 32 % and 34 % (according to the reinforcement ratio of the slabs). Using the punching shear expressions, the predicted increment of the concentrated load capacity $F_{predicted,punching}$ was 22 % for all tests. Therefore, both one-way shear expressions and punching shear expressions captured well, on average, the observed behavior for loads closer to the support. The larger enhancements predicted with the one-way shear expressions, regardless of the effective shear width decrease varying a_v/d_l from 2 to 1, occur because the relation $1/\beta_{arching}$ factor increases by 100 %.

In this study, these deviations from the tendencies identified can be attributed to the complex interaction between the shear failure mechanisms and the local yielding of the flexural reinforcements, which may trigger different failure mechanisms for some tests. For instance, the cracking pattern at the slab sides of L1-N ($a_v/d_l = 1$) indicated a shear-compression failure (Fig. 19). At this point, it is important to note that the arching action would increase the ultimate capacity mainly for tests subjected to shear-compression failures and not flexural-shear. However, extensive flexural cracking between the load and the support can reach the struts and disturb the contribution of arching action. Besides, the reinforcement yielding may limit the shear transfer between the load and the support because the tensile stress in the reinforcement reaches a yileding plateau, limiting the contribution of the concrete compression zone.

5.2. Effect of the ratio a/l_{span}

When the span length between the support decreases (increasing the ratio a/l_{span}), the proportion between the loads that go to the closer and far support becomes less uneven (Fig. 21) and the flexural demand decreases. It follows from statics that the reaction at the support close to the load decreases when a/l_{span} increases. The opposite behavior occurs for the reaction at the support farther away from the load. According to the Eurocode expressions, no change in the predicted sectional shear and punching capacity would be expected in such cases. For such cases, the bending moments at the front and back sides of the load decrease ($m_{E,x1}$ and $m_{E,x2}$) when the ratio a/l_{span} increases. In addition, the distance between contraflexure points in the side x_2 also decreases ($r_{s,x2}$). Therefore, based on the principles of the Critical Shear Crack Theory [28,48], a decrease of the slab rotations ψ and an increase in the punching capacity would be expected by increasing the ratio a/l_{span}, according to the following expression:

$$\psi_{ij} = 1.2 \cdot \frac{r_{s,ij}}{d_{avg}} \cdot \frac{f_y}{E_s} \cdot \left(\frac{m_{E,ij}}{m_{R,i}}\right)^{3/2}, i = \{x, y\} \text{ and } j = \{1, 2\} \quad (33)$$

Fig. 21 shows how the tested loads F_{test} and V_{test} vary as a function of the load position in terms of the ratio a/l_{span}. Tests with the same shear slenderness a_v/d_l but with a lower span between the supports were compared. Fig. 22 shows that a different behavior was observed according to the ratio a_v/d_l. For the tests with the load closer to the support and subject to arching action (L1-N to L1-S and L2-N to L2-S), decreasing the span length (and consequently increasing the ratio a/l_{span}) increased the tested capacities. Besides, this increase was more significant in the tests with a lower longitudinal reinforcement ratio (L1-N to L1-S).

In the tests with $a_v/d_l = 2$ (L2 and L5) and $a_v/d_l = 3$ (L3 and L6), most tests presented a decrease in the tested loads at failure by decreasing the span length (and consequently increasing a/l_{span}). The only exception occurred for the pair of tests L6-N to L6-S, which presented an increase in the tested loads by increasing the ratio a/l_{span}.

In summary, these results show that: (i) for loads with possible arching action, increasing the ratio a/l_{span} tends to increase the tested resistance; (ii) for load positions where arching action is hampered, the final resistance tends to decrease by increasing the ratio a/l_{span}. Theoretically, the fan struts between the load and the support may explain these different results. When arching action is possible, the fan of struts also improves the load that is transferred along the load's lateral sides, not only the load that goes through the front side. In other words, the arching action also improves the distribution of shear stresses in the transverse direction, in a similar effect to increase the effective shear width when arching action is possible. At larger distances from the load to the support, arching action is not possible, and the behavior of the

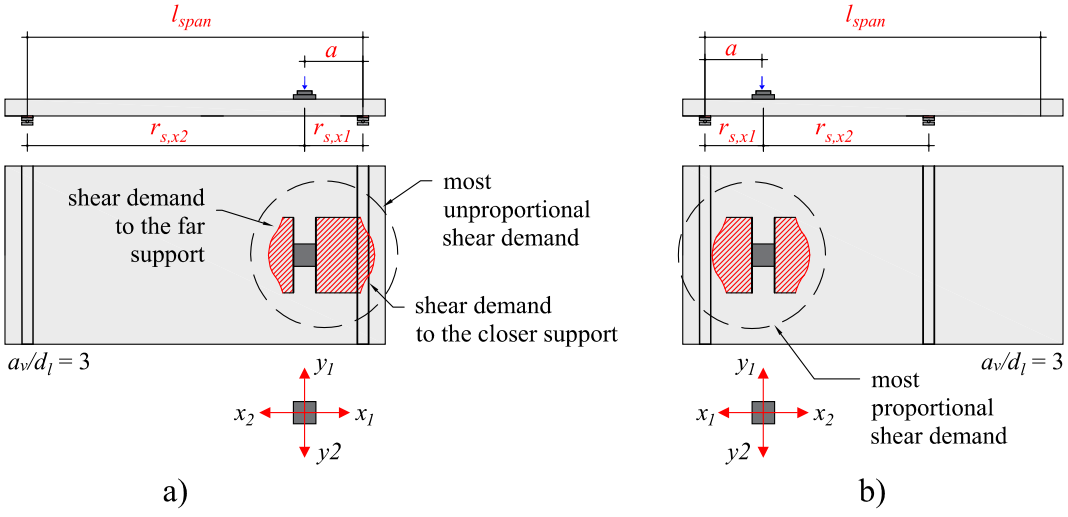

Fig. 21. Sketch of redistribution of shear forces at the front and back sides of the load according to the ratio a/l_{span}: (a) position of the first tests; (b) position of the second tests.

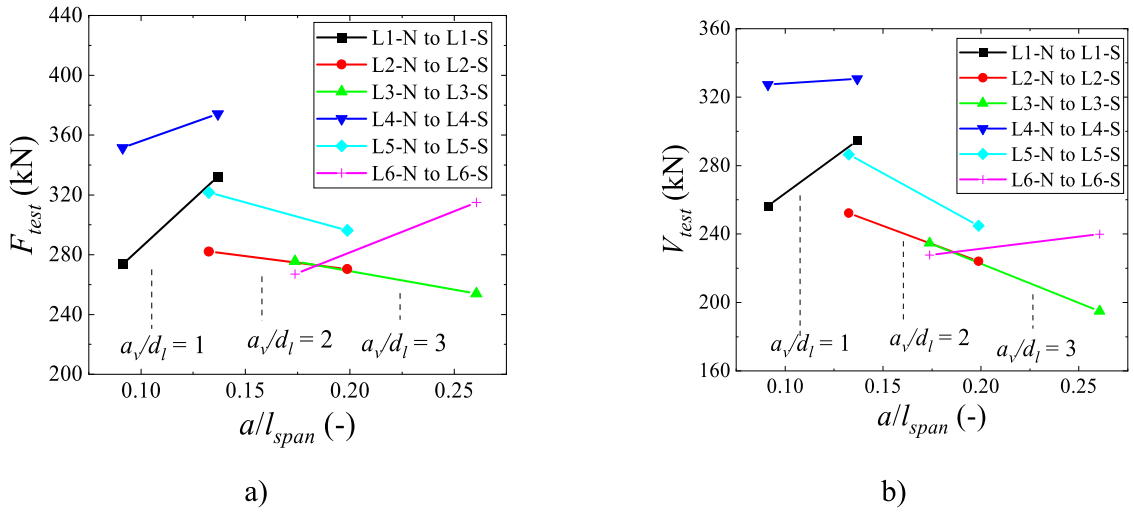

Fig. 22. Influence of load position in terms of the ratio a/l_{span}: (a) on tested peak loads F_{test} and (b) on calculated shear forces V_{test}.

structure is more complex: while the CSCT predicts an increase in the punching capacity when decreasing the span length, the most proportional shear demand around the load may trigger failures at lower load levels. This effect occurs because under a proportional shear demand around the load, the failure may be triggered at the weaker point around the load and not only at the region in the front side of the load, but further studies on this phenomenon are required.

6. Comparison between tested and predicted resistances

6.1. Flexural capacity predictions

Table 4 shows a comparison between tested and predicted resistances using the expressions from three collapse mechanisms (Fig. 4). Table 4 shows that, as expected based on previous studies [13], collapse mechanism 2 was the most critical one (providing the most conservative predictions for all slabs). On average, collapse mechanism 2 also fits better the tested resistances compared to other mechanisms. The average ratio between tested and predicted resistances $F_{test}/F_{flex,mech2}$ with mechanism 2 was 1.23, with a coefficient of variation of 15.4 %. The most conservative predictions of mechanism 2 occurs mainly because the reinforcement ratio in the transverse direction is considerably lower than the one applied in the longitudinal direction (0.44 % compared to 0.99 % and 1.32 %). In addition, the length of the yield line in the longitudinal direction is much lower than the one in the transverse direction. Consequently, the flexural capacity along this yield line is significantly lower.

6.2. One-way shear and punching capacity predictions

Table 5 shows the comparison between tested and predicted resistances (F_{test}/F_{pred}) using the shear, punching shear and flexural capacity calculations. Besides, Table 5 also shows the results using the Extended Strip Model [29], which combines characteristics from each mechanism in a single approach. In Table 5, the self-weight was considered in all calculations to determine F_{pred} for each mechanism. Fig. 23 shows the calculated effective shear width for one-way shear and the shear resisting control perimeter for each position of the tests. Regarding the predictions of flexural capacity, only the results from mechanism 2 are described since they provide the best accuracy compared to the tested results.

Column #8 shows that the predictions of the failure load were quite conservative for all tests, even considering the arching action for loads close to the support and an increase in the predicted effective shear width with the increase of the shear slenderness. The average ratio between tested and predicted resistances ($F_{test}/F_{predic,shear}$) was 1.70, with a coefficient of variation equal to 17.4 %. The causes for the conservativism in the results are: (i) not considering the enhanced transverse shear distribution for loads close to the support, which increases the effective shear width for loads benefitting from arching action [7] and (ii) the use of the one-way shear factor $C_{Rc,test}$ calibrated from beam tests [2]. Alternatively, the predictions of one-way shear capacity could

Table 4
Comparison between tested and predicted resistances using yield line analyses.

Ref-Teste	l_{span} (m)	a_v/d_l (-)	F_{test} (kN)	$F_{flex.mech1}$ (kN)	$F_{flex,mech2}$ (kN)	$F_{flex,mech3}$ (kN)	$\frac{F_{test}}{F_{flex.mech1}}$	$\frac{F_{test}}{F_{flex,mech2}}$	$\frac{F_{test}}{F_{flex.mech3}}$	CYLM[1]
L1-N	**3**	1	273.5	715.8	253.0	500.3	0.38	1.08	0.55	2
L2-N	**3**	2	282.1	574.0	255.1	358.5	0.49	1.11	0.79	2
L3-N	**3**	3	275.4	500.8	257.4	285.4	0.55	1.07	0.97	2
L1-S	**2**	1	332.1	673.8	211.0	530.1	0.49	1.57	0.63	2
L2-S	**2**	2	270.4	535.4	216.5	391.8	0.50	1.25	0.69	2
L3-S	**2**	3	253.9	466.4	223.0	322.8	0.54	1.14	0.79	2
L4-N	**3**	1	351.5	885.4	268.5	670.0	0.40	1.31	0.52	2
L5-N	**3**	2	321.6	696.4	271.3	480.9	0.46	1.19	0.67	2
L6-N	**3**	3	267.0	598.8	274.4	383.4	0.45	0.97	0.70	2
L4-S	**2**	1	374.1	852.4	235.4	708.7	0.44	1.59	0.53	2
L5-S	**2**	2	296.3	667.9	242.8	524.3	0.44	1.22	0.57	2
L6-S	**2**	3	314.8	575.9	251.5	432.3	0.55	1.25	0.73	2
		AVG	–	–	–	–	0.47	1.23	0.68	–
		COV (%)	–	–	–	–	11.9 %	15.4 %	19.3 %	–

[1] Most Critical Yield Line Mechanisms for the evaluated slab.

Table 5
Comparison between tested and predicted resistances according to different failure mechanisms and the ESM [29]. Note: PFM: predicted failure mechanism; S = one-way shear as wide beam; F = flexure.

#1	#2	#3	#4	#5	#6	#7	#8	#9	#10	#11	#12
Test	l_{span} **(m)**	a_v/d_l **(-)**	F_{test} (kN)	$F_{pred,shear}$ (kN)	$F_{pred,punching}$ (kN)	$F_{flex,mech2}$ (kN)	$\frac{F_{test}}{F_{pred,shear}}$	$\frac{F_{test}}{F_{pred,punc}}$	$\frac{F_{test}}{F_{flex,mech2}}$	**PFM**	$\frac{F_{test}}{F_{pred}}$
Details				***CEN*** $\beta_{arching}$	***CEN*** $\beta_{arching}$	–	***CEN*** $\beta_{arching}$	***CEN*** $\beta_{arching}$	***YLM***		***ESM*** [29]
L1-N	**3**	1	273.5	188.9	301.4	253.0	1.45	0.91	1.08	S	1.00
L2-N	**3**	2	282.1	125.0	234.4	255.1	2.26	1.20	1.11	S	1.33
L3-N	**3**	3	275.4	161.3	234.9	257.4	1.71	1.17	1.07	S	1.29
L1-S	**2**	1	332.1	198.9	301.4	211.0	1.67	1.10	1.57	S	1.20
L2-S	**2**	2	270.4	135.4	234.4	216.5	2.00	1.15	1.25	S	1.26
L3-S	**2**	3	253.9	180.3	234.9	223.0	1.41	1.08	1.14	S	1.17
L4-N	**3**	1	351.5	227.0	344.7	268.5	1.55	1.02	1.31	S	1.08
L5-N	**3**	2	321.6	150.8	268.1	271.3	2.13	1.20	1.19	S	1.29
L6-N	**3**	3	267.0	194.5	268.6	274.4	1.37	0.99	0.97	S	1.06
L4-S	**2**	1	374.1	239.0	344.7	235.4	1.57	1.09	1.59	F	1.14
L5-S	**2**	2	296.3	163.3	268.1	242.8	1.81	1.11	1.22	S	1.18
L6-S	**2**	3	314.8	217.4	268.6	251.5	1.45	1.17	1.25	S	1.23
						AVG	1.70	1.10	1.23		1.19
						COV (%)	17.4 %	8.2 %	15.4 %		8.7 %

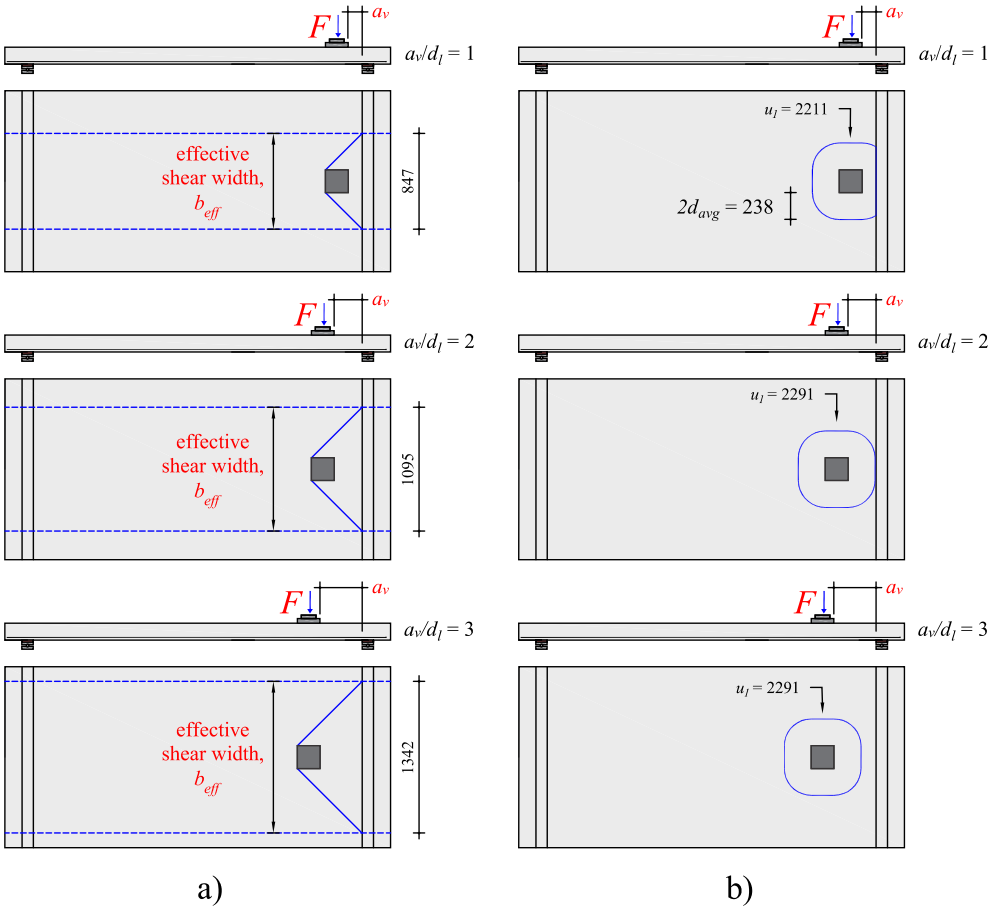

Fig. 23. (a) Determination of the effective shear width for one-way shear resistance analyses according to the French practice [21]; (b) determination of the shear resisting control perimeter according to the Brazilian and European design codes. Note: all dimensions in mm.

be enhanced if considering the improved unitary shear capacity for slabs under concentrated loads, and the actual shear demand v_E calculated aided by linear elastic finite element analyses, such as suggested in Henze et al. [2]. However, it is important to mention that the enhanced shear capacity $v_{R,shear}$, in this case, would not be related to the arching action, but to the capacity of the lateral distribution of the shear forces.

The predictions of ultimate capacity with the punching shear expressions (column #9), on the other hand, provided the most accurate predictions compared to the tested loads. The average ratio $F_{test}/F_{pred,punch}$ was 1.10 with a coefficient of variation of 8.2 %. In practice, these results also fit well with the observed failure mechanism of the tests, which started with punching before one-way shear at the slab sides occurred.

Comparing the predictions of one-way shear, punching shear and flexural capacity, one can realize the shortcomings that may appear when one of the expressions used is not properly calibrated. Although

the punching capacity predictions presented a lower error when compared to the test results, the theoretical governing failure mechanism (based on the predictions) would almost always be one-way shear. This conclusion occurs because the one-way shear approach provides the lowest predicted resistance between the three failure mechanisms considered (compare columns #5, #6 and #7).

In column #12, it can be seen that the Extended Strip Model [29] provided the best predictions, with an average ratio $F_{test}/F_{pred,punching}$ of 1.19 and a coefficient of variation equal to 8.7 %. At this point, this result can be explained by the fact that Extended Strip Model considers in a systematic way the load capacity of the slabs assuming reinforcement yielding around the load, which was verified in the tests. In addition, the average ratio $F_{test}/F_{pred,punching}$ of 1.19 is in line with the expectation that a lower-bound-plasticity-based model underestimates the capacity by about 20 % as a result of the assumptions inherent to using a lower-bound-plasticity-based method.

7. Discussions

Most previous publications in the field of one-way slabs under concentrated loads focused on conditions in which the shear and punching capacity are lower than the slab's flexural capacity [1,2,6,8–10]. These studies contributed to a better understanding of the problem when no local yielding of the flexural reinforcement occurs at failure. In this study, one-way slabs were tested to identify if and how local reinforcement yielding influences the behavior of slabs failing by shear. Compared to previous studies that also reported some reinforcement yielding at failure [49,50], we tried to improve the following aspects in the testing: (i) the load was applied following a displacement control, which allowed us to evaluate the post-peak behavior from the tested slabs (smooth or sharp decrease of the measured load on failure and residual resistance level after the first failure mechanism); (ii) the reinforcement strains in the longitudinal and transverse directions around the load were measured and evaluated together to show the shear redistribution after the development of the first failure mechanism; (iii) the cracking pattern of all slabs was provided in detail, showing the cracking pattern at the bottom side, top side and lateral side of the slabs.

The results indicated that after local reinforcement yielding of the slabs, the load can increase further until another failure mechanism occurs (punching shear or the one-way shear). In such cases, the final failure is brittle (see, for example, the force × displacement graph from test L3-N). As the ESM combines principles from the one-way shear and two-way shear mechanisms under the condition of reinforcement yielding, its use allows for predicting an accurate failure load when the slabs are subjected to local reinforcement yielding and conservative estimations when no reinforcement yielding is expected (since the real unitary shear capacity will be higher than the ones that assume reinforcement yielding at the strips).

In other tests, such as L1-N ($a_v/d_l = 1$), one could expect a brittle failure mechanism due to the smaller distance from the load to the support and the predominant direct shear transfer from the load towards the support by struts [1]. However, a smooth drop in the measured load was observed in such a test (see Fig. 13a). For slabs, this can be explained based on the fan of struts carrying the load [1]. When the full capacity of the main strut is reached, this strut will fail, but the load is redistributed laterally to struts that carry less load. This shear redistribution makes the failure of slabs less brittle compared to beams failing by shear compression [51]. In the case of beams or slabs loaded over the entire width, failing by flexure-shear or shear-compression, the one-way shear crack commonly develops suddenly along the entire width because of the most homogeneous distribution of shear stresses along the width.

In addition to the less brittle nature of the failure, another aspect draws our attention for test L1-N ($a_v/d_l = 1$): the applied load at failure was almost the same for L2-N ($a_v/d_l = 2$). For this test, an increase in the failure load was expected due to the decrease of the shear slenderness (a_v/d_l from 2 to 1) and, hence, the increase of arching action [1,23]. One possible explanation is that extensive flexural cracking occurred (see the bottom view in Fig. 16) due to the smaller slab thickness compared to other tests from the literature [1,2,6] and the smaller reinforcement ratio compared to slab L4. Such flexural cracks may have weakened the strut area and disabled the arching action. Therefore, the enhancement in the shear capacity for loads close to the support due to direct load transfer may be disturbed by local reinforcement yielding or extensive flexural cracking. A similar phenomenon was observed for deep beams with relatively low reinforcement ratios designed to fail in flexure ($d_l >$ 1000 mm and $\rho_l < 0.5$ %) [52]. In these experiments, sudden shear failures occurred due to the extensive flexural cracking and size effect in shear. However, further studies on the link between reinforcement yielding and shear-compression failures are necessary to address this observation.

In this study, an important evaluation commonly not performed was also added: the comparison between the ultimate concentrated loads predicted $F_{predicted}$ by one-way shear mechanisms, two-way shear mechanisms (punching) [2,8,10] and flexure. A close look into the comparisons between tested and predicted resistances also indicates an interesting point (Table 5). Although the predictions of punching capacity ($F_{test}/F_{pred,punching}$) fit the test results better, the theoretical failure mechanism was not predicted correctly. This mismatch occurs because the failure load $F_{predicted}$ for one-way shear was lower than that predicted for punching and flexure (the ratio $F_{test}/F_{pred,shear} > F_{test}/F_{pred,punching}$ and $F_{test}/F_{pred,shear} > F_{test}/F_{flex,mech2}$ for most tests, and consequently $F_{pred,shear} < F_{pred,punching}$ and $F_{pred,shear} < F_{flex,mech2}$). In practice, these results have two undesirable shortcomings: (i) for the design of new structures, the designer would need to change some aspects of the project to increase the one-way shear capacity over the flexural capacity due to the overly conservative prediction of one-way shear capacity (making the building more costly); (ii) for an existing structure, such predictions could lead to erroneous conclusions about the safety margins or about the governing failure mode and required strengthening actions, for instance. Therefore, the derivation of more accurate approaches to predict the one-way shear capacity of such slabs is also important, and these approaches are currently being developed [5,38].

In this study, we addressed the problem using mainly analytical expressions based on current European code provisions, yield line analyses and the ESM. This choice was motivated mainly because such approaches are the ones more frequently employed in the first assessment/scanning of databanks of bridges, following the principles of the Level of Approximation I in the current fib Model Code 2010 [46], when a large number of existing structures needs to be quickly rated, or when a first sketch of the structure is being developed. Because of this, simplified and conservative models are welcome at these stages. However, the following limitations of the applied methods shall be considered: (i) the use of code provisions such as the current Eurocode [53] does not allow consider the strain effect in the unitary shear capacity of reinforced concrete, well established in mechanical-based models such as in the Critical Shear Crack Theory for one-way shear or punching shear [28,47]; (ii) despite one of the yield line mechanisms tested (mechanism 2) provided reasonable levels of accuracy when compared to the tested loads, its extension to other slabs may need to be checked carefully since the yield line approach depends on the capacity of redistribution of the load as the steel starts to yield, and may vary significantly according to the boundary conditions and reinforcement layout; (iii) the Extended Strip Model is a lower bound solution. Therefore, it will provide more conservative results for slabs without reinforcement yielding, being recommended use only for the first assessment stages. To allow the most precise estimations of the shear demand and resistance (for one-way shear or punching shear), the use of finite element analyses combined or not with refined mechanical-based shear models are considered as a suitable alternative [2,8,44,45].

8. Conclusions

In this study, the failure mechanism of one-way slabs under concentrated loads with some local reinforcement yielding is studied. The load–displacement graphs, cracking pattern and reinforcement strains were monitored during the tests. Analytical predictions with the current European code expressions [53] and the Extended Strip Method [29] were performed and compared to those observed in the experiments. Besides, different failure mechanisms were considered in the predictions. The following conclusions can be drawn:

- One-way slabs under concentrated loads fail in a complex way when reinforcement yielding takes place. The resistance enhancement and shear compression failure expected for slabs with loads close to the support may not be achieved due to excessive flexural cracking between the load and the support (test L1-N to L2-N). Such a flexural crack can damage the struts and disable the expected arching action. Besides, brittle failure mechanisms can also occur after large reinforcement yielding due to a wide beam shear failure (test L3-N).
- Shear redistribution can occur around the load after punching and activate a secondary failure mechanism of one-way shear visible at the slab sides, called wide beam shear failure. In this study, such redistribution was attributed mainly to the relatively high reinforcement ratio applied in the transverse direction ($\rho_t = 0.44$ %) and the relation between the slab width and load size $b_{slab}/l_{load} = 8$.
- Combining the predictions of ultimate capacity (concentrated loads) that would cause a one-way shear failure or a punching failure in tested slabs, a conservative determination is achieved with the European design codes [53]. The punching capacity predictions were more accurate for predicting the maximum load on the tested slabs with local reinforcement yielding.
- The Extended Strip Model stands out as a solution to predict the ultimate capacity of reinforced concrete slabs under concentrated loads, especially when the slabs are subjected to some local reinforcement yielding at failure.
- The predictions of the ultimate capacity of the tested slabs with yield line analyses can present good levels of accuracy when the appropriate collapse mechanism is used, and the slabs present local reinforcement yielding, even when yielding is not observed over the full slab width or span length. In this study, the collapse mechanism that assumes yield lines between the center of the support and the load along the transverse reinforcement led to the best predictions (collapse mechanism 2).
- Comparing the predictions of one-way shear capacity, punching shear capacity and flexural capacity, erroneous conclusions about the safety margins and governing failure mechanism may occur when using current code approaches. In this study, despite the predictions of punching capacity fitting well with the test results, the ultimate capacity predicted with the one-way shear expressions was overly conservative. The predicted failure mode was almost always the one-way shear and not punching or flexure. Therefore, adjustments in the one-way shear expressions for slabs under concentrated loads are required to avoid such mistakes.

CRediT authorship contribution statement

Alex M.D. de Sousa: Conceptualization, Methodology, Software, Validation, Formal analysis, Investigation, Resources, Data curation, Writing – original draft, Writing – review & editing, Visualization. **Eva O.L. Lantsoght:** Conceptualization, Methodology, Investigation, Data curation, Writing – original draft, Writing – review & editing, Supervision. **Mounir K. El Debs:** Resources, Writing – review & editing, Supervision, Project administration, Funding acquisition.

Declaration of Competing Interest

The authors declare that they have no known competing financial interests or personal relationships that could have appeared to influence the work reported in this paper.

Data availability

Data will be made available on request.

Acknowledgement

The authors acknowledge the financial support provided by the São Paulo Research Foundation (FAPESP), grant number #2018/21573-2, grant number #2019/20092-3 and grant number #2021/13916-0; and by Brazilian National Council for Scientific and Technological Development (CNPq), grant number #303438/2016-9.

References

[1] Lantsoght EOL, van der Veen C, Walraven JC. Shear in one-way slabs under concentrated load close to support. ACI Struct J 2013;110:275–84. https://doi.org/10.14359/51684407.
[2] Henze L, Rombach GA, Harter M. New approach for shear design of reinforced concrete slabs under concentrated loads based on tests and statistical analysis. Eng Struct 2020;219:110795. https://doi.org/10.1016/j.engstruct.2020.110795.
[3] Bui TT, Limam A, Nana WSA, Ferrier E, Bost M, Bui Q-B. Evaluation of one-way shear behaviour of reinforced concrete slabs: experimental and numerical analysis. Eur J Environ Civ Eng 2017:1–27. https://doi.org/10.1080/19648189.2017.1371646.
[4] Fernández PG, Marí A, Oller E. Theoretical prediction of the shear strength of reinforced concrete slabs under concentrated loads close to linear supports. Struct Infrastruct Eng 2021:1–14. https://doi.org/10.1080/15732479.2021.1988990.
[5] de Sousa AMD, Lantsoght EOL, Yang Y, el Debs MK. Extended CSDT model for shear capacity assessments of bridge deck slabs. Eng Struct 2021;234:111897. https://doi.org/10.1016/j.engstruct.2021.111897.
[6] Reißen K, Classen M, Hegger J. Shear in reinforced concrete slabs-Experimental investigations in the effective shear width of one-way slabs under concentrated loads and with different degrees of rotational restraint. Struct Concr 2018;19:36–48. https://doi.org/10.1002/suco.201700067.
[7] de Sousa AMD, Lantsoght EOL, el Debs MK. Shear and Punching Capacity Predictions for One-Way Slabs under Concentrated Loads Considering the Transition between Failure Mechanisms. Buildings 2023;13:434. https://doi.org/10.3390/buildings13020434.
[8] Natário F, Fernández Ruiz M, Muttoni A. Shear strength of RC slabs under concentrated loads near clamped linear supports. Eng Struct 2014;76:10–23. https://doi.org/10.1016/j.engstruct.2014.06.036.
[9] Bui TT, Abouri S, Limam A, NaNa WSA, Tedoldi B, Roure T. Experimental investigation of shear strength of full-scale concrete slabs subjected to concentrated loads in nuclear buildings. Eng Struct 2017;131:405–20. https://doi.org/10.1016/j.engstruct.2016.10.045.
[10] Halvonik J, Vidaković A, Vida R. Shear Capacity of Clamped Deck Slabs Subjected to a Concentrated Load. J Bridg Eng 2020;25:04020037. https://doi.org/10.1061/(ASCE)BE.1943-5592.0001564.
[11] Gayed RB, Peiris C, Ghali A. Flexure-induced punching of concrete flat plates. Special Publication 2017;315:73–99.
[12] Widianto BO, Jirsa JO. Two-Way Shear Strength of Slab-Column Connections: Reexamination of ACI 318 Provisions. ACI Struct J 2009;106:160–70. https://doi.org/10.14359/56354.
[13] Belletti B, Damoni C, Hendriks MAN, De Boer A. Analytical and numerical evaluation of the design shear resistance of reinforced concrete slabs. Struct Concr 2014;15:317–30. https://doi.org/10.1002/suco.201300069.
[14] ACI Committee 318. Building Code Requirements for Structural Concrete (ACI 318-19) 2019:988.
[15] Hawkins NM, Ospina CE. Effect of slab flexural reinforcement and depth on punching strength. In: ACI-Fib international symposium: punching shear of structural concrete slabs (special publication) 2017;315:117–40.
[16] de Ferreira MP, Sacramento PVP, Lima Neto AF, Teixeira MR, de Oliveira DRC. Punching strength of RC slabs with asymmetric point loads. Acta Scientiarum - Technol 2016;38:71–80. https://doi.org/10.4025/actascitechnol.v38i1.27305.
[17] CEN. EN 1992-1-1: Eurocode 2: design of concrete structures-part 1-1: General rules and rules for buildings. EN 1992-1-1:2005; 2005.
[18] Regan PE. Shear resistance of members without shear reinforcement; proposal for CEB model code MC90; 1987:1–28.
[19] Konig G, Fischer J. Model uncertainties concerning design equations for the shear capacity of concrete members without shear reinforcement. In: CEB, editor. In CEB Bulletin 224, Model Uncertainties and Concrete Barrier for Environmental Protection, Lausanne, Switzerland: 1995, p. 49–100.

[20] Lantsoght EOL, van der Veen C, de Boer A, Walraven J. Proposal for the extension of the Eurocode shear formula for one-way slabs under concentrated loads. Eng Struct 2015;95:16–24. https://doi.org/10.1016/j.engstruct.2015.03.055.

[21] FD P 18-717. Eurocode 2 - Calcul des structures en béton - Guide d'application des normes NF EN 1992 2013.

[22] Coin A, Thonier H. Essais sur le cisaillement des dalles en beton arme. Annales du batiment et des travaux publics 2007:7–16.

[23] Sousa AMD, El Debs MK. Shear strength analysis of slabs without transverse reinforcement under concentrated loads according to ABNT NBR 6118:2014. IBRACON Structures and Materials Journal 2019;12:658–93. https://doi.org/10.1590/s1983-41952019000300012.

[24] Lantsoght EOL, van der Veen C, Walraven JC, de Boer A. Database of wide concrete members failing in shear. Mag Concr Res 2015;67:33–52. https://doi.org/10.1680/macr.14.00137.

[25] Bairán JM, Menduiña R, Marí A, Cladera A. Shear strength of non-slender reinforced concrete beams. ACI Struct J 2020:277–90. https://doi.org/10.14359/51721369.

[26] Natário F. Static and fatigue shear strength of reinforced concrete slabs under concentrated loads near linear support. PhD Thesis (Docteur ès Sciences), École Polytechnique Fédérale de Lausanne, 2015. doi: 10.5075/epfl-thesis-6670.

[27] Regan PE. Shear resistance of concrete slabs at concentrated loads close to supports. London, UK: Polytechnic of Central; 1982.

[28] Muttoni A. Punching shear strength of reinforced concrete slabs without transverse reinforcement. ACI Struct J 2008;105:440–50. https://doi.org/10.14359/19858.

[29] Lantsoght EOL, van der Veen C, de Boer A. Extended Strip Model for slabs subjected to load combinations. Eng Struct 2017;145:60–9. https://doi.org/10.1016/j.engstruct.2017.05.012.

[30] Alexander SDB, Simmonds SH. Bond model for concentric punching shear. ACI Struct J 1992;89:325–34. https://doi.org/10.14359/3246.

[31] ACI Committee 318. Building code requirements for structural concrete (ACI 318-14) and commentary 2014;11:6858.

[32] Limam S, Nana WSA, Bui TT, Limam A, Abouri S. Experimental investigation and analytical calculations on shear strength of full-scale RC slabs with shear reinforcement for nuclear power plants. Nucl Eng Des 2017;324:143–57. https://doi.org/10.1016/j.nucengdes.2017.08.035.

[33] Borghi TM, Oliveira LAM, el Debs ALH, Beck AT. Desempenho de Pontes Rurais com o avanço agrícola dos Rodotrens canavieiros - Análise baseada em Confiabilidade Estrutural. XII Congresso Brasileiro de Pontes e Estruturas. Congresso Virtual 2021.

[34] Prefeitura de Araras. Mais duas pontes são instaladas na zona rural de Araras 2015. https://araras.sp.gov.br/noticias/15901.

[35] Prefeitura de Extrema. 20ª ponte de aduelas de concreto está sendo finalizada na Zona Rural 2020. https://www.extrema.mg.gov.br/noticias/20a-ponte-de-aduelas-de-concreto-esta-sendo-finalizada-na-zona-rural/.

[36] Concrenorte - Pré Moldados e Construtora. Como são fabricadas as pontes rurais de concreto? n.d. https://concrenorte.com.br/como-sao-fabricadas-as-pontes-rurais-de-concreto/.

[37] Adam V, Classen M, Hillebrand M, Hegger J. Shear in continuous slab segments without shear reinforcement under distributed loads. Proceedings of the fib Symposium 2019 - Concrete - Innovations in Materials, Design and Structures, Krakow, Poland: 2019.

[38] de Sousa AMD, Lantsoght EOL, El Debs MK. Transition between shear and punching in reinforced concrete slabs: review and predictions with ACI code expressions. ACI Struct J 2023;120. https://doi.org/10.14359/51738350.

[39] Lantsoght EOL, van der Veen C, Walraven JC, de Boer A. Experimental investigation on shear capacity of reinforced concrete slabs with plain bars and slabs on elastomeric bearings. Eng Struct 2015;103:1–14. https://doi.org/10.1016/J.ENGSTRUCT.2015.08.028.

[40] Fernández PG, Marí A, Oller E. Punching-shear strength of reinforced concrete slabs subjected to unidirectional in-plane tensile forces. Struct Concr 2020:1–16. https://doi.org/10.1002/suco.202000112.

[41] Reiβen K. Zum Querkrafttragverhalten von einachsig gespannten Stahlbetonplatten ohne Querkraftbewehrung unter Einzellasten. Doctor of Engineering. PhD Thesis (Doctor of Engineering), Faculty of Civil Engineering, RWTH Aachen University, 2016.

[42] Reineck K-H, Bentz EC, Fitik B, Kuchma DA, Bayrak O. ACI-DAfStb database of shear tests on slender reinforced concrete beams without stirrups. ACI Struct J 2013;110:867–76. https://doi.org/10.14359/51685839.

[43] Rombach G, Latte S. Querkrafttragfähigkeit Von Fahrbahnplatten Ohne Querkraftbewehrung. Beton- Stahlbetonbau 2009;104:642–56. https://doi.org/10.1002/best.200900029.

[44] Cantone R, Fernández Ruiz M, Muttoni A. Shear force redistributions and resistance of slabs and wide beams. Struct Concr 2021:suco.202100127. doi: 10.1002/suco.202100127.

[45] Cantone R, Setiawan A, Fernández Ruiz M, Muttoni A. Characterization of shear deformations in reinforced concrete members without shear reinforcement. Eng Struct 2022;257:113910. https://doi.org/10.1016/J.ENGSTRUCT.2022.113910.

[46] Fédération Internationale du Béton (fib). fib Model Code for Concrete Structures 2010. vol. 1–2. Lausanne, Switzerland: Ernst & Sohn - fédération internationale du béton, Bulletin 65; 2012.

[47] Muttoni A, Fernandez RM. Shear strength of members without transverse reinforcement as function of critical shear crack width. ACI Struct J 2008;105:163–72. https://doi.org/10.14359/19731.

[48] Sagaseta J, Tassinari L, Fernández Ruiz M, Muttoni A. Punching of flat slabs supported on rectangular columns. Eng Struct 2014;77:17–33. https://doi.org/10.1016/j.engstruct.2014.07.007.

[49] Regan PE, Rezai-Jorabi H. Shear resistance of one-way slabs under concentrated loads. ACI Struct J 1988;85:150–7. https://doi.org/10.14359/2704.

[50] Ferreira M de P. Experimental analysis of one-way reinforced concrete flat slabs in axis or non-axis-symmetric punching shear (in Portuguese: Análise experimental de lajes lisas unidirecionais de concreto armado ao puncionamento simétrico ou assimétrico). Masters' thesis, Universidade Federal do Pará, 2006.

[51] de Sousa AMD, Lantsoght EOL, El Debs MK. One-way shear strength of wide reinforced concrete members without stirrups. Struct Concr 2020:1–25. https://doi.org/10.1002/suco.202000034.

[52] Yang Y, van der Ham H, Naaktgeboren M. Shear capacity of RC slab structures with low reinforcement ratio – an experimental approach. Lisbon, Lisbon, Portugal; 2021.

[53] CEN. EN 1992-1-1: Eurocode 2: design of concrete structures-part 1-1: General rules and rules for buildings. EN 1992-1-1:2004; 2004.